Journal of Computational Physics 229 (2010) 4934–4951

Contents lists available at ScienceDirect

Journal of Computational Physics

journal homepage: www.elsevier.com/locate/jcp

A hybrid finite/boundary element method for periodic structures on non-periodic meshes using an interior penalty formulation for Maxwell's equations

Seung-Cheol Lee [a], Vineet Rawat [b], Jin-Fa Lee [c,*]

[a] Ansoft Corporation, Pittsburgh, United States
[b] SLAC, Stanford University, United States
[c] ElectroScience Laboratory, ECE Department, The Ohio State University, United States

ARTICLE INFO

Article history:
Received 4 December 2009
Received in revised form 22 February 2010
Accepted 14 March 2010
Available online 21 March 2010

Keywords:
Periodic structure
Interior penalty
Finite elements
Boundary elements

ABSTRACT

This paper presents a hybrid finite element/boundary element (FEBE) method for periodic structures. Periodic structures have been efficiently analyzed by solving for a single unit cell utilizing Floquet's theorem. However, most of the previous works require periodic meshes to properly impose the boundary conditions on the outer surfaces of the unit cell. To alleviate this restriction, the interior penalty method is adopted and implemented in this work. Also, the proper treatment of the boundary element part is addressed to account for the non-conformity of the boundary element mesh. Another ingredient of this work is the use of the efficient boundary element computation, accelerated by the Ewald transformation for the calculation of the periodic Green's function. Finally, the method is validated through examples which are discretized without the constraint of a periodic mesh.

1. Introduction

Recent interest in analyzing and designing large finite antenna arrays [1,2], frequency selective surfaces (FSS) [3], and metamaterials [4,5] speak volumes to the need for a robust and efficient numerical method for arbitrary and inhomogeneous periodic structures in 3D. The development of numerical methods for analyzing arbitrary 3-dimensional periodic structures is nothing new. Much existing literature has thoroughly addressed this issue [6–12], including the hybridization of finite and boundary element methods using the Ewald transform to quickly compute the periodic Green's function [9]. However, most of the work on modeling periodic structures relies on the availability of periodic meshes. Although this constraint may not seem to be a great burden in many problem geometries, the relief of such a constraint still contributes greatly to the flexibility of applying computer codes to periodic structures. This attribute has been the focus of a few recent publications on using non-periodic meshes for analyzing periodic structures [11,12].

However, a hybridization of finite element and boundary element methods on non-periodic meshes has not yet been available, and that leads us to propose a possible solution to accomplish a successful hybridization without mesh constraints. To account for non-periodic meshes, the interior penalty approach [13–17] is utilized in this work to enforce proper periodic boundary conditions across non-matching grids.

The early efforts to support non-conforming finite elements using the interior penalty method can be found in [13–15]. These works were for elliptic and parabolic equations, but recent study of the interior penalty method for Maxwell's

* Corresponding author. Tel.: +1 614 292 7270; fax: +1 614 292 7297.
E-mail addresses: lee.1802@osu.edu (S.-C. Lee), vrawat@slac.stanford.edu (V. Rawat), lee.1863@osu.edu, jinlee@ece.osu.edu (J.-F. Lee).

0021-9991/$ - see front matter © 2010 Elsevier Inc. All rights reserved.
doi:10.1016/j.jcp.2010.03.014

equations [16,17] reveals the applicability of the method to Maxwell's regime. The common approach is to weakly enforce the Dirichlet condition at each element level, but in the present work, we enforce the weak continuity only where the non-matching grid occurs. More precisely, the boundary conditions at the side walls of the unit cell are treated through the interior penalty approach. Moreover, the formulation presented in this paper enforces the Robin transmission conditions found in domain decomposition methods [18,19].

Our interest in this work includes analysis of the radiation and scattering properties of doubly periodic structures, which requires proper truncation of the computational geometry. The finite element method (FEM) often incorporates local truncation techniques such as a simple absorbing boundary condition (ABC) [20] or perfectly matched layer (PML) [21]. Although computationally efficient, those boundary conditions alter the physical character of the problem. The truncation boundaries are basically absorbers which often fail to represent the outer space correctly. Particularly, these approaches require the truncation boundaries to be convex in shape. On the other hand, the boundary element method (BEM) accurately projects the infinite outer space onto the truncation surface as a boundary condition. Therefore, we use the BEM in this work for the truncation of a unit cell. In addition, the Ewald transformation [9,22] is adopted for the efficient computation of the periodic Green's function. The non-conformity of the boundary elements between unit cells is also addressed and a possible solution is presented.

2. Formulation

2.1. Notation

The tangential surface trace π_τ and twisted tangential surface trace γ_τ are first defined as

$$\begin{aligned}\pi_\tau(\mathbf{v}_i) &:= \mathbf{n}_i \times (\mathbf{v}_i \times \mathbf{n}_i),\\ \gamma_\tau(\mathbf{v}_i) &:= \mathbf{n}_i \times \mathbf{v}_i,\end{aligned} \tag{1}$$

where $\mathbf{n}_i$ is the outgoing normal on the surface Γ_i, and the subscript i indicates the location of the evaluation, namely,

$$\mathbf{v}_i := \mathbf{v}|_{\Gamma_i}, \tag{2}$$

The associated jump operators on Γ are given by

$$\begin{aligned}[\![\mathbf{v}]\!]_\gamma &:= \mathbf{n} \times \mathbf{v}^- - \mathbf{n} \times \mathbf{v}^+,\\ [\![\mathbf{v}]\!]_\pi &:= \pi_\tau(\mathbf{v}^-) - \pi_\tau(\mathbf{v}^+),\end{aligned} \tag{3}$$

where the superscripts + and − represents exterior and interior sides of the surface Γ, respectively. The volume and surface sesqulinear forms are given by

$$\begin{aligned}(\mathbf{w},\mathbf{v})_\Omega &:= \int_\Omega \mathbf{w}^* \cdot \mathbf{v} dV,\\ \langle \mathbf{w},\mathbf{v}\rangle_\Gamma &:= \int_\Gamma \mathbf{w}^* \cdot \mathbf{v} dS.\end{aligned} \tag{4}$$

2.2. Boundary value problem

The problem that we are interested in solving in this paper is depicted in Fig. 1. It corresponds to infinite periodic structures, such as infinite antenna phased arrays, frequency selective surfaces (FSS), and metamaterials, residing in unbounded free space. As shown in the figure, we have divided the entire geometry into interior and exterior regions, Ω and Ω_{ex}, respec-

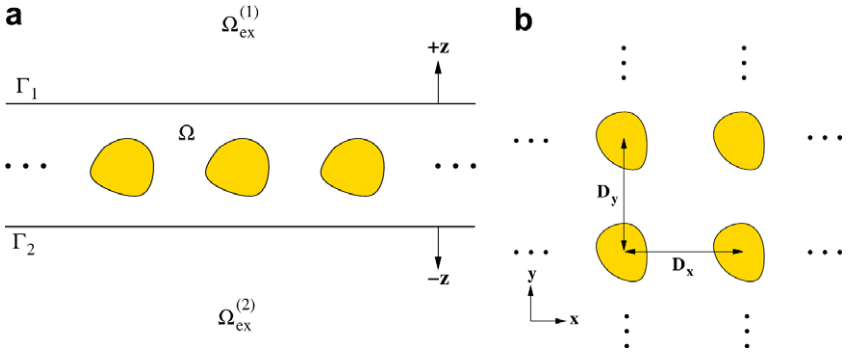

Fig. 1. Generic infinite periodic structure: (a) side view and (b) top view.

tively, and the exterior region is further decomposed into $\Omega_{ex}^{(1)}$ and $\Omega_{ex}^{(2)}$. Let $\mathbf{E}$ denote the scattered and total electric field in the exterior and interior regions, and since we are interested in solving both electromagnetic wave radiation and scattering with infinite periodic structures, we shall state our boundary value problem (BVP) formally as:

$$\nabla \times \frac{1}{\mu_r} \nabla \times \mathbf{E} - k_0^2 \epsilon_r \mathbf{E} = -jk_0 \eta \mathbf{J}^{\text{imp}}, \quad \text{in } \Omega, \tag{5}$$

$$\nabla \times \nabla \times \mathbf{E}_i - k_0^2 \mathbf{E}_i = 0, \quad \text{in } \Omega_{ex}^{(i)} \quad i = 1, 2, \tag{6}$$

$$[\![\mathbf{E}]\!]_\pi = \pi_\tau(\mathbf{E}^{\text{inc}}), \quad \text{on } \Gamma_i \quad i = 1, 2, \tag{7}$$

$$[\![\frac{1}{\mu_r} \nabla \times \mathbf{E}]\!]_\gamma = \gamma_\tau(\nabla \times \mathbf{E}^{\text{inc}}), \quad \text{on } \Gamma_i \quad i = 1, 2, \tag{8}$$

where ϵ_r and μ_r are the relative permittivity and permeability, respectively, k_0 is the wavenumber in free space, η is the intrinsic impedance, $\mathbf{J}^{\text{imp}}$ is the impressed current, and $\mathbf{E}^{\text{inc}}$ represents the incident electric field. Note also that, in order for the BVP to be formulated as an infinite periodic problem, we need to insist that material properties, μ_r and ϵ_r, and excitations, $\mathbf{J}^{\text{imp}}$ and $\mathbf{E}^{\text{inc}}$, are all periodic functions of the form $f(\mathbf{r} + mD_x\mathbf{x} + nD_y\mathbf{y}) = \alpha_x^m \alpha_y^n f(\mathbf{r})$, with $\alpha_x = \exp^{-jk_0 \sin\vartheta \cos\varphi D_x}$ and $\alpha_y = \exp^{-jk_0 \sin\vartheta \sin\varphi D_y}$, for any integers m and n. The spherical coordinates ϑ and φ are used to describe the scanning direction of a phased array or the propagation direction of an incident plane wave. Additionally, the scattered field $\mathbf{E}_i$ in the exterior region, $\Omega_{ex}^{(i)}$, will have to satisfy the radiation condition as $|z| \to \infty$. Hence, the scattered electric field, $\mathbf{E}_i$, and its curl, $\nabla \times \mathbf{E}_i$, in $\Omega_{ex}^{(i)}$, can be expressed in terms of surface currents (or surface traces), $\mathbf{J}_i := \gamma_\tau(\mathbf{H}_i)$ and $\mathbf{M}_i := -\gamma_\tau(\mathbf{E}_i)$, through the following representation formulae:

$$\mathbf{E}_i(\mathbf{r}) = -jk_0 \eta \mathbf{A}(\mathbf{J}_i)(\mathbf{r}) - \frac{j\eta}{k_0} \nabla \Phi(\mathbf{J}_i)(\mathbf{r}) + \mathbf{C}(\mathbf{M}_i)(\mathbf{r}), \quad \mathbf{r} \in \Omega_{ex}^{(i)} \quad i = 1, 2, \tag{9}$$

$$\nabla \times \mathbf{E}_i(\mathbf{r}) = -k_0^2 \mathbf{A}(\mathbf{M}_i)(\mathbf{r}) - \nabla \Phi(\mathbf{M}_i)(\mathbf{r}) + jk_0 \eta \mathbf{C}(\mathbf{J}_i)(\mathbf{r}), \quad \mathbf{r} \in \Omega_{ex}^{(i)} \quad i = 1, 2. \tag{10}$$

Similarly, we have also the representation formulae for the total field,

$$\mathbf{E}_i^{total}(\mathbf{r}) = -jk_0 \eta \mathbf{A}(\mathbf{J}_i^{total})(\mathbf{r}) - \frac{j\eta}{k_0} \nabla \Phi(\mathbf{J}_i^{total}(\mathbf{r}) + \mathbf{C}(\mathbf{M}_i^{total})(\mathbf{r}), \quad \mathbf{r} \in \Omega_{ex}^{(i)} \quad i = 1, 2, \tag{11}$$

$$\mathbf{H}_i^{total}(\mathbf{r}) = -\frac{jk_0}{\eta} \mathbf{A}(\mathbf{M}_i^{total})(\mathbf{r}) - \frac{j}{k_0 \eta} \nabla \Phi(\mathbf{M}_i^{total}(\mathbf{r}) - \mathbf{C}(\mathbf{J}_i^{total})(\mathbf{r}), \quad \mathbf{r} \in \Omega_{ex}^{(i)} \quad i = 1, 2. \tag{12}$$

Obviously, $\mathbf{E}_i^{total} = \mathbf{E}_i + \mathbf{E}_i^{inc}, \mathbf{H}_i^{total} = \mathbf{H}_i + \mathbf{H}_i^{inc}, \mathbf{J}_i^{total} = \mathbf{J}_i + \mathbf{J}_i^{inc}$ and, $\mathbf{M}_i^{total} = \mathbf{M}_i + \mathbf{M}_i^{inc}$.

The potential operators used in (9) and (10) are defined by:

$$\mathbf{A}(\mathbf{v}_i)(\mathbf{r}) := \int_{\Gamma_i^+} G(\mathbf{r}, \mathbf{r}') \mathbf{v}_i(\mathbf{r}') dS', \quad \mathbf{r} \in \Omega_{ex}^{(i)} \quad i = 1, 2, \tag{13}$$

$$\Phi(\mathbf{v}_i)(\mathbf{r}) := \int_{\Gamma_i^+} G(\mathbf{r}, \mathbf{r}') \nabla'_\tau \cdot \mathbf{v}_i(\mathbf{r}') dS', \quad \mathbf{r} \in \Omega_{ex}^{(i)} \quad i = 1, 2, \tag{14}$$

$$\mathbf{C}(\mathbf{v}_i)(\mathbf{r}) := \int_{\Gamma_i^+} \nabla' G(\mathbf{r}, \mathbf{r}') \times \mathbf{v}_i(\mathbf{r}') dS', \quad \mathbf{r} \in \Omega_{ex}^{(i)} \quad i = 1, 2 \tag{15}$$

and $G(\mathbf{r}, \mathbf{r}') = \frac{\exp^{-jk_0|\mathbf{r}-\mathbf{r}'|}}{4\pi|\mathbf{r}-\mathbf{r}'|}$ is the fundamental solution of the scalar Helmholtz equation in 3D. Moreover, we employ notations Γ_i^+ and Γ_i^- to denote the exterior and interior sides of the boundary surface Γ_i, respectively. The notation $\nabla_\tau \cdot$ is used to denote the surface divergence operator. We call $\mathbf{A}$ and Φ the single-layered vector and scalar potentials, respectively whereas the integral $\mathbf{C}$ is called the double-layered potential (see [23] for details). Taking the limit of $\mathbf{r}(\in \Omega_{ex}^{(i)}) \to \bar{\mathbf{r}}(\in \Gamma_i)$, the three potentials in (13)–(15) become

$$\lim_{\mathbf{r}(\in \Omega_{ex}^{(i)}) \to \bar{\mathbf{r}}(\in \Gamma_i)} \mathbf{A}(\mathbf{v}_i)(\mathbf{r}) = \mathbf{A}(\mathbf{v}_i)(\bar{\mathbf{r}}) = \int_{\Gamma_i^+} G(\bar{\mathbf{r}}, \mathbf{r}') \mathbf{v}_i(\mathbf{r}') dS', \tag{16}$$

$$\lim_{\mathbf{r}(\in \Omega_{ex}^{(i)}) \to \bar{\mathbf{r}}(\in \Gamma_i)} \Phi(\mathbf{v}_i)(\mathbf{r}) = \Phi(\mathbf{v}_i)(\bar{\mathbf{r}}) = \int_{\Gamma_i^+} G(\bar{\mathbf{r}}, \mathbf{r}') \nabla'_\tau \cdot \mathbf{v}_i(\mathbf{r}') dS', \tag{17}$$

$$\lim_{\mathbf{r}(\in \Omega_{ex}^{(i)}) \to \bar{\mathbf{r}}(\in \Gamma_i)} \mathbf{C}(\mathbf{v}_i)(\mathbf{r}) = -\frac{1}{2} \mathbf{v}_i \times \mathbf{n}_i + pv \int_{\Gamma_i^+} \nabla' G(\bar{\mathbf{r}}, \mathbf{r}') \times \mathbf{v}_i(\mathbf{r}') dS' = -\frac{1}{2} \mathbf{v}_i \times \mathbf{n}_i + \mathbf{C}(\mathbf{v}_i)(\bar{\mathbf{r}}). \tag{18}$$

In (18), The notation $\mathbf{C}(\mathbf{v}_i)(\bar{\mathbf{r}})$ is understood as $\mathbf{C}(\mathbf{v}_i)(\bar{\mathbf{r}}) = pv \int_{\Gamma_i^+} \nabla' G(\bar{\mathbf{r}}, \mathbf{r}') \times \mathbf{v}_i(\mathbf{r}') dS'$ and pv stands for principal value.

To derive surface integral equations (SIEs) for surface traces, we take the representation formulae, letting $\mathbf{r}(\in \Omega_{ex}^{(i)}) \to \bar{\mathbf{r}}(\in \Gamma_i)$, and apply the limits (16)–(18) to result in

$$\frac{1}{2}\mathbf{M}_i^+(\bar{\mathbf{r}}) = jk_0\eta\gamma_\tau(\mathbf{A}(\mathbf{J}_i^+)(\bar{\mathbf{r}})) + \frac{j\eta}{k_0}\gamma_\tau(\nabla_\tau\Phi(\mathbf{J}_i^+)(\bar{\mathbf{r}})) - \gamma_\tau(\mathbf{C}(\mathbf{M}_i^+)(\bar{\mathbf{r}})) \quad \bar{\mathbf{r}} \in \Gamma_i, \tag{19}$$

$$\frac{1}{2}\mathbf{J}_i^+(\bar{\mathbf{r}}) = -\frac{jk_0}{\eta}\gamma_\tau(\mathbf{A}(\mathbf{M}_i^+)(\bar{\mathbf{r}})) - \frac{j}{k_0\eta}\gamma_\tau(\nabla_\tau\Phi(\mathbf{M}_i^+)(\bar{\mathbf{r}})) - \gamma_\tau(\mathbf{C}(\mathbf{J}_i^+)(\bar{\mathbf{r}})) \quad \bar{\mathbf{r}} \in \Gamma_i. \tag{20}$$

Moreover, we can apply the same limit to (12) and results in

$$\frac{1}{2}\mathbf{J}_i^{+,t}(\bar{\mathbf{r}}) = \mathbf{J}_i^{inc}(\bar{\mathbf{r}}) - \frac{jk_0}{\eta}\gamma_\tau(\mathbf{A}(\mathbf{M}_i^{+,t})(\bar{\mathbf{r}})) - \frac{j}{k_0\eta}\gamma_\tau(\nabla_\tau\Phi(\mathbf{M}_i^{+,t})(\bar{\mathbf{r}})) - \gamma_\tau(\mathbf{C}(\mathbf{J}_i^{+,t})(\bar{\mathbf{r}}))\bar{\mathbf{r}} \in \Gamma_i, \tag{21}$$

where the superscript t denotes the total field.

However, the two SIEs can be further simplified by noting $\gamma_\tau(\mathbf{C}(\mathbf{v}_i))(\bar{\mathbf{r}}) = 0$ for planar Γ_i, which is the case here. We shall use the second of these two SIEs to form the needed Dirichlet to Neumann (DtN) condition. Since $\mathbf{J}_i^+ = \mathbf{J}_i^- - \mathbf{J}_i^{\text{inc}}$ and $\mathbf{M}_i^+ = \mathbf{M}_i^- - \mathbf{M}_i^{\text{inc}}$, after substitution into (20), we have

$$\frac{1}{2}\mathbf{J}_i^-(\bar{\mathbf{r}}) = -\frac{jk_0}{\eta}\gamma_\tau(\mathbf{A}(\mathbf{M}_i^-)(\bar{\mathbf{r}})) - \frac{j}{k_0\eta}\gamma_\tau(\nabla_\tau\Phi(\mathbf{M}_i^-)(\bar{\mathbf{r}})) + \mathbf{J}_i^{\text{inc}}. \tag{22}$$

In reaching (22), we have employed the following relation.

$$\frac{1}{2}\mathbf{J}_i^{\text{inc}}(\bar{\mathbf{r}}) = \frac{jk_0}{\eta}\gamma_\tau(\mathbf{A}(\mathbf{M}_i^{\text{inc}})(\bar{\mathbf{r}})) + \frac{j}{k_0\eta}\gamma_\tau(\nabla_\tau\Phi(\mathbf{M}_i^{\text{inc}})(\bar{\mathbf{r}})). \tag{23}$$

Eq. (23) is the direct consequence of (21) for the special case where the scattered fields are zero, and therefore, the total fields are the same as the incident fields.

Finally, we are able to write the BVP only with respect to the interior region, Ω, as:

$$\nabla \times \frac{1}{\mu_r}\nabla \times \mathbf{E} - k_0^2\epsilon_r\mathbf{E} = -jk_0\eta\mathbf{J}^{\text{imp}}, \quad \text{in } \Omega \tag{24}$$

$$\gamma_\tau(\mathbf{E}) = 0, \quad \text{on } \Gamma_{\text{PEC}} \tag{25}$$

$$\frac{1}{2}\gamma_\tau\left(\frac{1}{\mu_r}\nabla \times \mathbf{E}|_{\Gamma_i}\right) = -k_0^2\gamma_\tau(\mathbf{A}(\mathbf{M}_i)) - \gamma_\tau(\nabla\Phi(\mathbf{M}_i)) + \gamma_\tau(\nabla \times \mathbf{E}^{\text{inc}}|_{\Gamma_i}). \quad \text{on } \Gamma_i \quad i = 1, 2. \tag{26}$$

2.3. BVP for unit cell

For an infinite periodic structure, one can consider only the unit cell, $\widetilde{\Omega}$, as the problem domain as shown in Fig. 2. In this case, the DtN mapping can be written using the field of the unit cell as

$$\frac{1}{2}\gamma_\tau\left(\frac{1}{\mu_r}\nabla \times \mathbf{E}|_{\Gamma_i}\right) = -k_0^2\gamma_\tau(\mathbf{A}_{\text{p}}(\mathbf{M}_i^-)) - \gamma_\tau(\nabla\Phi_{\text{p}}(\mathbf{M}_i^-)) + \gamma_\tau(\nabla \times \mathbf{E}^{\text{inc}}|_{\Gamma_i}), \tag{27}$$

with

$$\begin{aligned}\mathbf{A}_{\text{p}}(\mathbf{v}) &= \int_{\Gamma_i^+} G_{\text{p}}(\mathbf{r}, \mathbf{r}')\mathbf{v}(\mathbf{r}')dS', \\ \Phi_{\text{p}}(\mathbf{v}) &= \int_{\Gamma_i^+} G_{\text{p}}(\mathbf{r}, \mathbf{r}')\nabla_\tau \cdot (\mathbf{v}(\mathbf{r}'))dS'.\end{aligned} \tag{28}$$

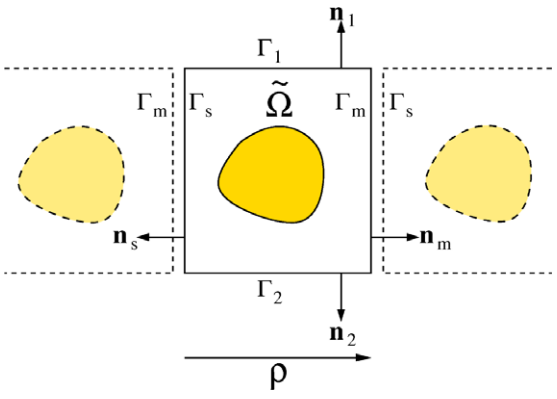

Fig. 2. Unit cell of a generic periodic structure.

In (28), the periodic Green's function G_p is used to represent the repetition of the surface $\overline{\Gamma_i}$, which is the restriction of the surface Γ_i in the unit cell, and the evaluation of $G_p(\mathbf{r},\mathbf{r}')$ using the Ewald transformation will be briefly given in Section 2.6.

The boundary conditions on Γ_m and Γ_s, the master and slave boundaries, respectively, should also be established. Through the Floquet theorem, the relationship between $\mathbf{E}_m(\equiv \pi_\tau(\mathbf{E}|_{\Gamma_m}))$ and $\mathbf{E}_s(\equiv \pi_\tau(\mathbf{E}|_{\Gamma_s}))$ can be described as

$$\mathbf{E}_m = \alpha \mathbf{E}_s, \tag{29}$$

where the phase shift from Γ_s to Γ_m in the unit cell is expressed in α as

$$\alpha = e^{-j\mathbf{k}_t\cdot\boldsymbol{\rho}}, \tag{30}$$

with

$$\mathbf{k}_t = k_0 \sin\vartheta\cos\varphi\hat{\mathbf{x}} + k_0\sin\vartheta\sin\varphi\hat{\mathbf{y}}. \tag{31}$$

As mentioned earlier, the spherical coordinates ϑ and φ are used to describe the scanning direction of a phased array or the propagating direction of an incident plane wave. The Dirichlet and Neumann boundary conditions on Γ_m or Γ_s can now be described as

$$\begin{aligned} &\pi_\tau(\mathbf{E}_m) = \alpha\pi_\tau(\mathbf{E}_s),\\ &\gamma_\tau\left(\frac{1}{\mu_r}\nabla\times\mathbf{E}_m\right) = -\alpha\gamma_\tau\left(\frac{1}{\mu_r}\nabla\times\mathbf{E}_s\right). \end{aligned} \tag{32}$$

Finally, we state the BVP within the unit cell formally

$$\nabla\times\frac{1}{\mu_r}\nabla\times\mathbf{E} - k_0^2\epsilon_r\mathbf{E} = -jk_0\eta\mathbf{J}^{\text{imp}}, \quad \text{in } \widetilde{\Omega}, \tag{33}$$

$$\gamma_\tau(\mathbf{E}) = 0, \quad \text{on } \Gamma_{\text{PEC}}, \tag{34}$$

$$\pi_\tau(\mathbf{E}_m) = \alpha\pi_\tau(\mathbf{E}_s), \quad \text{on } \Gamma_p, \tag{35}$$

$$\gamma_\tau\left(\frac{1}{\mu_r}\nabla\times\mathbf{E}_m\right) = -\alpha\gamma_\tau\left(\frac{1}{\mu_r}\nabla\times\mathbf{E}_s\right), \quad \text{on } \Gamma_p, \tag{36}$$

$$\frac{1}{2}\gamma_\tau\left(\frac{1}{\mu_r}\nabla\times\mathbf{E}|_{\overline{\Gamma_i}}\right) = -k_0^2\gamma_\tau(\mathbf{A}_p(\mathbf{M}_i^-)) - \gamma_\tau(\nabla\Phi_p(\mathbf{M}_i^-)) + \gamma_\tau(\nabla\times\mathbf{E}^{\text{inc}}|_{\overline{\Gamma_i}}), \quad \text{on } \overline{\Gamma_i}, \tag{37}$$

where Γ_p is introduced for the interface between the unit cells, and as a result Γ_m and Γ_s are either side of Γ_p.

2.4. Interior penalty formulation

2.4.1. General Galerkin weak statement

Before we move onto the Galerkin procedure, it would be beneficial to categorize the electromagnetic quantities into four forms as

0 - form (associated with point) ϕ,
1 - form (associated with length) $\mathbf{E},\mathbf{H}$,
2 - form (associated with area) $\mathbf{D},\mathbf{B},\mathbf{J},\mathbf{M}$,
3 - form (associated with volume) ρ.

From a physical point of view, a proper dual pairing results in an energy density (or power density) such as $\rho\phi, \mathbf{E}\cdot\mathbf{D}, \mathbf{H}\cdot\mathbf{B}, \mathbf{E}\cdot\mathbf{J}$ or $\mathbf{H}\cdot\mathbf{M}$. In the energy densities, one can easily find that a p form pairs with a 3-p form. The testing procedure herein will closely follow this rule.

As usual, the solution $\mathbf{E}$ resides in the function space $\mathbf{H}(curl,\widetilde{\Omega}) = \{\mathbf{v}|\mathbf{v},\nabla\times\mathbf{v}\in(L^2(\widetilde{\Omega}))^3\}$. To begin the interior penalty formulation, we start by stating that there will be four residuals associated with any given trial electric field $\mathbf{u}\in\mathbf{H}(curl,\widetilde{\Omega})$, based on the BVP. They are:

Residuals	Physical meanings	
$\mathbf{R}^{(1)}_{\widetilde{\Omega}}(\mathbf{u}) := \nabla\times\frac{1}{\mu_r}\nabla\times\mathbf{u} - k_0^2\epsilon_r\mathbf{u} + jk_0\eta\mathbf{J}^{\text{imp}}$	$-jk_0\eta\mathbf{J}^{err}$,	(38)
$\mathbf{R}^{(2)}_{\Gamma_p}(\mathbf{u}) := \pi_\tau(\mathbf{u}_m) - \alpha\pi_\tau(\mathbf{u}_s)$	$\mathbf{n}\times\mathbf{M}_p^{err}$,	(39)
$\mathbf{R}^{(3)}_{\Gamma_p}(\mathbf{u}) := \gamma_\tau\left(\frac{1}{\mu_r}\nabla\times\mathbf{u}_m\right) + \alpha\gamma_\tau\left(\frac{1}{\mu_r}\nabla\times\mathbf{u}_s\right)$	$-jk_0\eta\mathbf{J}_p^{err}$,	(40)
$\mathbf{R}^{(4)}_{\overline{\Gamma_i}}(\mathbf{u}) := \gamma_\tau\left(\frac{1}{\mu_r}\nabla\times\mathbf{u}_i\right) + 2k_0^2\gamma_\tau(\mathbf{A}_p(\mathbf{M}_i^{\mathbf{u}})) + 2\gamma_\tau(\nabla_\tau\Phi_p(\mathbf{M}_i^{\mathbf{u}})) - 2\gamma_\tau(\nabla\times\mathbf{E}_i^{\text{inc}})$	$-jk_0\eta\mathbf{J}_i^{err}$,	(41)

where $\mathbf{M}_i^{\mathbf{u}} = -\gamma_\tau(\mathbf{u}_i)$. The physical meanings of these four residuals, as indicated in (38)–(41), are: $\mathbf{R}^{(1)}_{\widetilde{\Omega}}(\mathbf{u})$ is the volume error current (multiplied by scalar coefficient $-jk_0\eta$) to support the difference between the trial electric field $\mathbf{u}$ and the exact

solution $\mathbf{E}$; $\mathbf{R}^{(2)}_{\Gamma_p}(\mathbf{u})$ and $\mathbf{R}^{(3)}_{\Gamma_p}(\mathbf{u})$ are the surface error magnetic current ($\mathbf{M}^{err}_p$ with a rotation $\mathbf{n}\times$) and the surface error electric current ($-jk_0\eta\mathbf{J}^{err}_p$) to maintain the discontinuities between the surface electric fields $\pi_\tau(\mathbf{u}_m)$ and $\alpha\pi_\tau(\mathbf{u}_s)$, and the surface magnetic fields $\gamma_\tau(\nabla\times\mathbf{u}|_{\Gamma_m})$ and $-\alpha\gamma_\tau(\nabla\times\mathbf{u}|_{\Gamma_s})$, on the periodic boundary, Γ_p, respectively. Similarly, the residual $\mathbf{R}^{(4)}_{\overline{\Gamma_i}}(\mathbf{u})$ on the mesh truncation boundary $\overline{\Gamma_i}$ has the physical meaning of $-jk_0\eta\mathbf{J}^{err}_i$, with $\mathbf{J}^{err}_i$ being the error surface current needed to support the discontinuity between $\gamma_\tau\left(\frac{1}{\mu_r}\nabla\times\mathbf{u}_i\right)$ and the exterior trace $\gamma_\tau(\nabla\times\mathbf{u}|_{\overline{\Gamma_i}^+})$, described by (8).

Hence, by following the power density argument presented earlier, we pair $\mathbf{R}^{(1)}_{\underset{\sim}{\Omega}}(\mathbf{u})$ with an arbitrary test electric field $\mathbf{v}\in\mathbf{H}(curl,\widetilde{\Omega})$, $\mathbf{R}^{(2)}_{\Gamma_p}(\mathbf{u})$ with the average test surface electric current, $\frac{1}{2}\left(\gamma_\tau\left(\frac{1}{\mu_r}\nabla\times\mathbf{v}_m\right)-\alpha\gamma_\tau\left(\frac{1}{\mu_r}\nabla\times\mathbf{v}_s\right)\right)$, $\mathbf{R}^{(3)}_{\Gamma_p}(\mathbf{u})$ with the average test surface electric field, $\frac{1}{2}(\pi_\tau(\mathbf{v}_m)+\alpha\pi_\tau(\mathbf{v}_s))$, and, lastly, $\mathbf{R}^{(4)}_{\overline{\Gamma_i}}(\mathbf{u})$ with the test surface electric field, $\pi_\tau(\mathbf{v}_i)$ to form inner products. By summing these inner products, weighted with different scalar coefficients (to be determined later), we are ready to formally state our Galerkin weak formulation:

Find $\mathbf{u}\in\mathbf{H}(curl,\widetilde{\Omega})$ such that

$$(\mathbf{v},\mathbf{R}^{(1)}_{\underset{\sim}{\Omega}}(\mathbf{u}))_{\underset{\sim}{\Omega}}+c_1\left\langle\frac{1}{2}\left(\gamma_\tau\left(\frac{1}{\mu_r}\nabla\times\mathbf{v}_m\right)-\alpha\gamma_\tau\left(\frac{1}{\mu_r}\nabla\times\mathbf{v}_s\right)\right),\mathbf{R}^{(2)}_{\Gamma_p}(\mathbf{u})\right\rangle_{\Gamma_p}+c_2\left\langle\frac{1}{2}(\pi_\tau(\mathbf{v}_m)+\alpha\pi_\tau(\mathbf{v}_s)),\mathbf{R}^{(3)}_{\Gamma_p}(\mathbf{u})\right\rangle_{\Gamma_p}$$
$$+\sum_{i=1}^{2}c_3\langle\pi_\tau(\mathbf{v}_i),\mathbf{R}^{(4)}_{\overline{\Gamma_i}}(\mathbf{u})\rangle_{\overline{\Gamma_i}}=0. \tag{42}$$

$\forall\mathbf{v}\in\mathbf{H}(curl,\widetilde{\Omega})$

The justification of the interior penalty formulation lies in the fact that each residual is tested either by independent testing functions or on different manifolds. For example, with $\mathbf{v}\in\mathbf{H}(curl,\widetilde{\Omega})$, we have

$$\begin{aligned}&\gamma_\tau\left(\frac{1}{\mu_r}\nabla\times\mathbf{v}_m\right)\in(L^2(\Gamma_m))^2\quad\text{and,}\\&\pi_\tau(\mathbf{v}_m)\in\mathbf{H}^{-\frac{1}{2}}(curl_\Gamma,\Gamma_m).\end{aligned} \tag{43}$$

By insisting Eq. (42) holds true for any vector testing function $\mathbf{v}\in\mathbf{H}(curl,\widetilde{\Omega})$, the resulting Euler–Lagrange equations recovers the original BVP (33)–(37). See Ref. [15] for details.

Moreover, in the interior penalty formulation, we are offered the possibility of including additional inner products, related to the jumps of electric and magnetic traces on the periodic boundary Γ_p. Namely, we may include

$$\langle\pi_\tau(\mathbf{v}_m)-\alpha\pi_\tau(\mathbf{v}_s),\frac{1}{Z_p}(\pi_\tau(\mathbf{u}_m)-\alpha\pi_\tau(\mathbf{u}_s))\rangle_{\Gamma_p}, \tag{44}$$

and

$$\langle\gamma_\tau\left(\frac{1}{\mu_r}\nabla\times\mathbf{v}_m\right)+\alpha\gamma_\tau\left(\frac{1}{\mu_r}\nabla\times\mathbf{v}_s\right),Z_p\left(\gamma_\tau\left(\frac{1}{\mu_r}\nabla\times\mathbf{u}_m\right)+\alpha\gamma_\tau\left(\frac{1}{\mu_r}\nabla\times\mathbf{u}_s\right)\right)\rangle_{\Gamma_p} \tag{45}$$

with $Z_p=\sqrt{\frac{\mu_{r,p}}{\epsilon_{r,p}}}$ indicating an average relative impedance for Γ_p, where $\mu_{r,p}$ and $\epsilon_{r,p}$ are the average relative permeability and permittivity on Γ_p, respectively. Again, (44) and (45) are of the physical significance of dissipation power density. Adding these two terms into (42), we have a very general Galerkin weak formulation for solving the BVP within the unit cell (33)–(37):

Find $\mathbf{u}\in\mathbf{H}(curl,\widetilde{\Omega})$ such that

$$(\mathbf{v},\mathbf{R}^{(1)}_{\underset{\sim}{\Omega}}(\mathbf{u}))_{\underset{\sim}{\Omega}}+c_1\left\langle\frac{1}{2}\left(\gamma_\tau\left(\frac{1}{\mu_r}\nabla\times\mathbf{v}_m\right)-\alpha\gamma_\tau\left(\frac{1}{\mu_r}\nabla\times\mathbf{v}_s\right)\right),\mathbf{R}^{(2)}_{\Gamma_p}(\mathbf{u})\right\rangle_{\Gamma_p}+c_2\left\langle\frac{1}{2}(\pi_\tau(\mathbf{v}_m)+\alpha\pi_\tau(\mathbf{v}_s)),\mathbf{R}^{(3)}_{\Gamma_p}(\mathbf{u})\right\rangle_{\Gamma_p}$$
$$+\sum_{i=1}^{2}c_3\langle\pi_\tau(\mathbf{v}_i),\mathbf{R}^{(4)}_{\overline{\Gamma_i}}(\mathbf{u})\rangle_{\overline{\Gamma_i}}+p\langle\pi_\tau(\mathbf{v}_m)-\alpha\pi_\tau(\mathbf{v}_s),\frac{1}{Z_p}(\pi_\tau(\mathbf{u}_m)-\alpha\pi_\tau(\mathbf{u}_s))\rangle_{\Gamma_p}$$
$$+q\left\langle\gamma_\tau\left(\frac{1}{\mu_r}\nabla\times\mathbf{v}_m\right)+\alpha\gamma_\tau\left(\frac{1}{\mu_r}\nabla\times\mathbf{v}_s\right),Z_p\left(\gamma_\tau\left(\frac{1}{\mu_r}\nabla\times\mathbf{u}_m\right)+\alpha\gamma_\tau\left(\frac{1}{\mu_r}\nabla\times\mathbf{u}_s\right)\right)\right\rangle_{\Gamma_p}=0. \tag{46}$$

$\forall\mathbf{v}\in\mathbf{H}(curl,\widetilde{\Omega})$

2.4.2. Choice of coefficients

In general, the choices of c_1,c_2,c_3, p and q can be determined via considerations of accuracy or convenience. The choice of c_3 in this work is due to the latter consideration, where we choose $c_3=-1$ to remove $\left\langle\pi_\tau(\mathbf{v}_i),\gamma_\tau\left(\frac{1}{\mu_r}\nabla\times\mathbf{u}_i\right)\right\rangle_{\overline{\Gamma_i}}$ which appears in the fourth inner product term of (46). To view this clearly, consider the inner products $(\mathbf{v},\mathbf{R}^{(1)}_{\underset{\sim}{\Omega}}(\mathbf{u}))_{\underset{\sim}{\Omega}}$ and $\langle\pi_\tau(\mathbf{v}_i),\mathbf{R}^{(4)}_{\overline{\Gamma_i}}(\mathbf{u})\rangle_{\overline{\Gamma_i}}$. After applying the Green's identities, $(\mathbf{v},\mathbf{R}^{(1)}_{\underset{\sim}{\Omega}}(\mathbf{u}))_{\underset{\sim}{\Omega}}$ becomes

$$(\mathbf{v},\mathbf{R}^{(1)}_{\underset{\sim}{\Omega}}(\mathbf{u}))_{\underset{\sim}{\Omega}} = (\nabla\times\mathbf{v},\frac{1}{\mu_r}\nabla\times\mathbf{u})_{\underset{\sim}{\Omega}} - k_0^2(\mathbf{v},\epsilon_r\mathbf{u})_{\underset{\sim}{\Omega}} + jk_0\eta(\mathbf{v},\mathbf{J}^{\mathrm{imp}})_{\underset{\sim}{\Omega}} + \left\langle \pi_\tau(\mathbf{v}_\mathrm{m}),\gamma_\tau\left(\frac{1}{\mu_r}\nabla\times\mathbf{u}_\mathrm{m}\right)\right\rangle_{\Gamma_\mathrm{m}} + \left\langle \pi_\tau(\mathbf{v}_\mathrm{s}),\gamma_\tau\left(\frac{1}{\mu_r}\nabla\times\mathbf{u}_\mathrm{s}\right)\right\rangle_{\Gamma_\mathrm{s}} + \sum_{i=1}^{2}\left\langle \pi_\tau(\mathbf{v}_i),\gamma_\tau\left(\frac{1}{\mu_r}\nabla\times\mathbf{u}_i\right)\right\rangle_{\overline{\Gamma_i}}. \tag{47}$$

Now expanding $\langle\pi_\tau(\mathbf{v}_i),\mathbf{R}^{(4)}_{\overline{\Gamma_i}}(\mathbf{u})\rangle_{\overline{\Gamma_i}}$,

$$\langle\pi_\tau(\mathbf{v}_i),\mathbf{R}^{(4)}_{\overline{\Gamma_i}}(\mathbf{u})\rangle_{\overline{\Gamma_i}} = \left\langle \pi_\tau(\mathbf{v}_i),\gamma_\tau\left(\frac{1}{\mu_r}\nabla\times\mathbf{u}_i\right)\right\rangle_{\overline{\Gamma_i}} + \langle\pi_\tau(\mathbf{v}_i),2k_0^2\gamma_\tau(\mathbf{A}_\mathrm{p}(\mathbf{M}_i^{\mathbf{u}}))\rangle_{\overline{\Gamma_i}} + \langle\pi_\tau(\mathbf{v}_i),2\gamma_\tau(\nabla_\tau\Phi_\mathrm{p}(\mathbf{M}_i^{\mathbf{u}}))\rangle_{\overline{\Gamma_i}} - \langle\pi_\tau(\mathbf{v}_i),2\gamma_\tau(\nabla\times\mathbf{E}_i^{\mathrm{inc}})\rangle_{\overline{\Gamma_i}}. \tag{48}$$

Obviously, by choosing $c_3=-1$, the inner product $\left\langle \pi_\tau(\mathbf{v}_i),\gamma_\tau\left(\frac{1}{\mu_r}\nabla\times\mathbf{u}_i\right)\right\rangle_{\overline{\Gamma_i}}$ will disappear.

The choice of c_1 and c_2 is due to consideration of symmetry in this work. However, symmetric matrix equations are obtained only when $\alpha=1$. Otherwise, the matrices will be neither symmetric nor hermitian due to the periodic Green's function. Nevertheless, our numerical experiments indicate that the choice of c_1 and c_2 herein results in the optimal rate of convergence, which will be shown later. To decide the coefficients, the second and the third inner products in (46) are expanded as

$$\begin{aligned}&\left\langle\frac{1}{2}\left(\gamma_\tau\left(\frac{1}{\mu_r}\nabla\times\mathbf{v}_\mathrm{m}\right)-\gamma_\tau\left(\frac{1}{\mu_r}\nabla\times\mathbf{v}_\mathrm{s}\right)\right),\pi_\tau(\mathbf{u}_\mathrm{m})-\pi_\tau(\mathbf{u}_\mathrm{s})\right\rangle_{\Gamma_\mathrm{p}}\\ &=\frac{1}{2}\left\langle\gamma_\tau\left(\frac{1}{\mu_r}\nabla\times\mathbf{v}_\mathrm{m}\right),\pi_\tau(\mathbf{u}_\mathrm{m})\right\rangle_{\Gamma_\mathrm{m}}-\frac{1}{2}\left\langle\gamma_\tau\left(\frac{1}{\mu_r}\nabla\times\mathbf{v}_\mathrm{m}\right),\pi_\tau(\mathbf{u}_\mathrm{s})\right\rangle_{\Gamma_\mathrm{p}}-\frac{1}{2}\left\langle\gamma_\tau\left(\frac{1}{\mu_r}\nabla\times\mathbf{v}_\mathrm{s}\right),\pi_\tau(\mathbf{u}_\mathrm{m})\right\rangle_{\Gamma_\mathrm{p}}\\ &\quad+\frac{1}{2}\left\langle\gamma_\tau\left(\frac{1}{\mu_r}\nabla\times\mathbf{v}_\mathrm{s}\right),\pi_\tau(\mathbf{u}_\mathrm{s})\right\rangle_{\Gamma_\mathrm{s}},\end{aligned} \tag{49}$$

$$\begin{aligned}&\left\langle\frac{1}{2}(\pi_\tau(\mathbf{v}_\mathrm{m})+\pi_\tau(\mathbf{v}_\mathrm{s})),\gamma_\tau\left(\frac{1}{\mu_r}\nabla\times\mathbf{u}_\mathrm{m}\right)+\gamma_\tau\left(\frac{1}{\mu_r}\nabla\times\mathbf{u}_\mathrm{s}\right)\right\rangle_{\Gamma_\mathrm{p}}\\ &=\frac{1}{2}\left\langle\pi_\tau(\mathbf{v})_\mathrm{m},\gamma_\tau\left(\frac{1}{\mu_r}\nabla\times\mathbf{u}_\mathrm{m}\right)\right\rangle_{\Gamma_\mathrm{m}}+\frac{1}{2}\left\langle\pi_\tau(\mathbf{v})_\mathrm{m},\gamma_\tau\left(\frac{1}{\mu_r}\nabla\times\mathbf{u}_\mathrm{s}\right)\right\rangle_{\Gamma_\mathrm{p}}+\frac{1}{2}\left\langle\pi_\tau(\mathbf{v})_\mathrm{s},\gamma_\tau\left(\frac{1}{\mu_r}\nabla\times\mathbf{u}_\mathrm{m}\right)\right\rangle_{\Gamma_\mathrm{p}}\\ &\quad+\frac{1}{2}\left\langle\pi_\tau(\mathbf{v})_\mathrm{s},\gamma_\tau\left(\frac{1}{\mu_r}\nabla\times\mathbf{u}_\mathrm{s}\right)\right\rangle_{\Gamma_\mathrm{s}},\end{aligned} \tag{50}$$

where $\alpha=1$ is already assumed. Examining (47), (49) and (50), it can be found that $c_1=1$ and $c_2=-1$ result in the following inner products on the periodic boundary:

$$\begin{aligned}&\frac{1}{2}\left\langle\gamma_\tau\left(\frac{1}{\mu_r}\nabla\times\mathbf{v}_\mathrm{m}\right),\pi_\tau(\mathbf{u}_\mathrm{m})\right\rangle_{\Gamma_\mathrm{m}}-\frac{1}{2}\left\langle\gamma_\tau\left(\frac{1}{\mu_r}\nabla\times\mathbf{v}_\mathrm{m}\right),\pi_\tau(\mathbf{u}_\mathrm{s})\right\rangle_{\Gamma_\mathrm{p}}-\frac{1}{2}\left\langle\gamma_\tau\left(\frac{1}{\mu_r}\nabla\times\mathbf{v}_\mathrm{s}\right),\pi_\tau(\mathbf{u}_\mathrm{m})\right\rangle_{\Gamma_\mathrm{p}}\\ &\quad+\frac{1}{2}\left\langle\gamma_\tau\left(\frac{1}{\mu_r}\nabla\times\mathbf{v}_\mathrm{s}\right),\pi_\tau(\mathbf{u}_\mathrm{s})\right\rangle_{\Gamma_\mathrm{s}}+\frac{1}{2}\left\langle\pi_\tau(\mathbf{v})_\mathrm{m},\gamma_\tau\left(\frac{1}{\mu_r}\nabla\times\mathbf{u}_\mathrm{m}\right)\right\rangle_{\Gamma_\mathrm{m}}-\frac{1}{2}\left\langle\pi_\tau(\mathbf{v})_\mathrm{m},\gamma_\tau\left(\frac{1}{\mu_r}\nabla\times\mathbf{u}_\mathrm{s}\right)\right\rangle_{\Gamma_\mathrm{p}}\\ &\quad-\frac{1}{2}\left\langle\pi_\tau(\mathbf{v})_\mathrm{s},\gamma_\tau\left(\frac{1}{\mu_r}\nabla\times\mathbf{u}_\mathrm{m}\right)\right\rangle_{\Gamma_\mathrm{p}}+\frac{1}{2}\left\langle\pi_\tau(\mathbf{v})_\mathrm{s},\gamma_\tau\left(\frac{1}{\mu_r}\nabla\times\mathbf{u}_\mathrm{s}\right)\right\rangle_{\Gamma_\mathrm{s}}\\ &=\frac{1}{2}\left\langle\gamma_\tau\left(\frac{1}{\mu_r}\nabla\times\mathbf{v}_\mathrm{m}\right)-\gamma_\tau\left(\frac{1}{\mu_r}\nabla\times\mathbf{v}_\mathrm{s}\right),\pi_\tau(\mathbf{u}_\mathrm{m})-\pi_\tau(\mathbf{u}_\mathrm{s})\right\rangle_{\Gamma_\mathrm{p}}\\ &\quad+\frac{1}{2}\left\langle\pi_\tau(\mathbf{v}_\mathrm{m})-\pi_\tau(\mathbf{v}_\mathrm{s}),\gamma_\tau\left(\frac{1}{\mu_r}\nabla\times\mathbf{u}_\mathrm{m}\right)-\gamma_\tau\left(\frac{1}{\mu_r}\nabla\times\mathbf{u}_\mathrm{s}\right)\right\rangle_{\Gamma_\mathrm{p}}.\end{aligned} \tag{51}$$

The symmetry is clearly observed in (51), where the jump of the surface electric field is paired with the average of the test surface electric current and the average of the surface electric current is paired with the jump of the test surface electric field. These pairs (with the same sign) can be easily found in symmetric interior penalty (SIP) methods [17,24].

Lastly, the parameters p and q can be chosen to weakly enforce "transmission conditions" (TCs) [18,19] on the periodic boundary, Γ_p. Following the study in [18,19], we set p and q to impose Robin type transmission conditions on Γ_p. Rearranging the terms relating Γ_p in (46), and using the previously chosen coefficients $c_1=1$, $c_2=-1$ and $c_3=-1$,

$$\left\langle \gamma_\tau\left(\frac{1}{\mu_r}\nabla\times\mathbf{v}_{\mathrm{m}}\right), (\pi_\tau(\mathbf{u}_{\mathrm{m}}) - \alpha\pi_\tau(\mathbf{u}_{\mathrm{s}})) + 2qZ_p\left(\gamma_\tau\left(\frac{1}{\mu_r}\nabla\times\mathbf{u}_{\mathrm{m}}\right) + \alpha\gamma_\tau\left(\frac{1}{\mu_r}\nabla\times\mathbf{u}_{\mathrm{s}}\right)\right)\right\rangle_{\Gamma_{\mathrm{m}}} = 0, \tag{52}$$

$$\left\langle \gamma_\tau\left(\frac{1}{\mu_r}\nabla\times\mathbf{v}_{\mathrm{s}}\right), (\pi_\tau(\mathbf{u}_{\mathrm{m}}) - \alpha\pi_\tau(\mathbf{u}_{\mathrm{s}})) - 2qZ_p\left(\gamma_\tau\left(\frac{1}{\mu_r}\nabla\times\mathbf{u}_{\mathrm{m}}\right) + \alpha\gamma_\tau\left(\frac{1}{\mu_r}\nabla\times\mathbf{u}_{\mathrm{s}}\right)\right)\right\rangle_{\Gamma_{\mathrm{s}}} = 0, \tag{53}$$

$$\left\langle \pi_\tau(\mathbf{v}_{\mathrm{m}}), \frac{2p}{Z_p}(\pi_\tau(\mathbf{u}_{\mathrm{m}}) - \alpha\pi_\tau(\mathbf{u}_{\mathrm{s}})) - \left(\gamma_\tau\left(\frac{1}{\mu_r}\nabla\times\mathbf{u}_{\mathrm{m}}\right) + \alpha\gamma_\tau\left(\frac{1}{\mu_r}\nabla\times\mathbf{u}_{\mathrm{s}}\right)\right)\right\rangle_{\Gamma_{\mathrm{m}}} = 0, \tag{54}$$

$$\left\langle \pi_\tau(\mathbf{v}_{\mathrm{s}}), \frac{2p}{Z_p}(\pi_\tau(\mathbf{u}_{\mathrm{m}}) - \alpha\pi_\tau(\mathbf{u}_{\mathrm{s}})) + \left(\gamma_\tau\left(\frac{1}{\mu_r}\nabla\times\mathbf{u}_{\mathrm{m}}\right) + \alpha\gamma_\tau\left(\frac{1}{\mu_r}\nabla\times\mathbf{u}_{\mathrm{s}}\right)\right)\right\rangle_{\Gamma_{\mathrm{s}}} = 0. \tag{55}$$

To enforce the Robin transmission conditions used in [19];

$$\gamma_\tau\left(\frac{1}{\mu_r}\nabla\times\mathbf{u}_{\mathrm{m}}\right) - \frac{jk_0}{Z_p}\pi_\tau(\mathbf{u}_{\mathrm{m}}) = -\alpha\gamma_\tau\left(\frac{1}{\mu_r}\nabla\times\mathbf{u}_{\mathrm{s}}\right) - \frac{jk_0}{Z_p}\alpha\pi_\tau(\mathbf{u}_{\mathrm{s}}), \tag{56}$$

$$\gamma_\tau\left(\frac{1}{\mu_r}\nabla\times\mathbf{u}_{\mathrm{s}}\right) - \frac{jk_0}{Z_p}\pi_\tau(\mathbf{u}_{\mathrm{s}}) = -\frac{1}{\alpha}\gamma_\tau\left(\frac{1}{\mu_r}\nabla\times\mathbf{u}_{\mathrm{m}}\right) - \frac{jk_0}{\alpha Z_p}\pi_\tau(\mathbf{u}_{\mathrm{m}}), \tag{57}$$

the coefficients p and q are chosen to be $p = \frac{jk_0}{2}$ and $q = -\frac{1}{2jk_0}$. Note that through (52)–(55) the transmission conditions (56) and (57) are tested twice by test surface electric current and test surface electric field, respectively. These testings enlarge the testing space into $(L^2(\Gamma_{\mathrm{p}}))^3$, which is desirable since the function space of (56) and (57) is also in $(L^2(\Gamma_{\mathrm{p}}))^3$.

Finally, (46) can be rewritten using the coefficients found in this section and the Green's identity as

$$\begin{aligned}
&(\nabla\times\mathbf{v}, \frac{1}{\mu_r}\nabla\times\mathbf{u})_{\widetilde{\Omega}} - k_0^2(\mathbf{v}, \epsilon_r\mathbf{u})_{\widetilde{\Omega}} + \frac{1}{2}\left\langle \gamma_\tau\left(\frac{1}{\mu_r}\nabla\times\mathbf{v}_{\mathrm{m}}\right) - \alpha\gamma_\tau\left(\frac{1}{\mu_r}\nabla\times\mathbf{v}_{\mathrm{s}}\right), \pi_\tau(\mathbf{u}_{\mathrm{m}}) - \alpha\pi_\tau(\mathbf{u}_{\mathrm{s}})\right\rangle_{\Gamma_{\mathrm{p}}} \\
&+ \frac{1}{2}\left\langle \pi_\tau(\mathbf{v}_{\mathrm{m}}) - \alpha\pi_\tau(\mathbf{v}_{\mathrm{s}}), \gamma_\tau\left(\frac{1}{\mu_r}\nabla\times\mathbf{u}_{\mathrm{m}}\right) - \alpha\gamma_\tau\left(\frac{1}{\mu_r}\nabla\times\mathbf{u}_{\mathrm{s}}\right)\right\rangle_{\Gamma_{\mathrm{p}}} + 2\sum_{i=1}^{2}\left\langle \pi_\tau(\mathbf{v}_i), \gamma_\tau(k_0^2\mathbf{A}_{\mathrm{p}}(\mathbf{M}_i^{\mathbf{u}}) + \nabla\Phi_{\mathrm{p}}(\mathbf{M}_i^{\mathbf{u}}))\right\rangle_{\overline{\Gamma_i}} \\
&+ \frac{jk_0}{2}\left\langle \pi_\tau(\mathbf{v}_{\mathrm{m}}) - \alpha\pi_\tau(\mathbf{v}_{\mathrm{s}}), \frac{1}{Z_p}(\pi_\tau(\mathbf{u}_{\mathrm{m}}) - \alpha\pi_\tau(\mathbf{u}_{\mathrm{s}}))\right\rangle_{\Gamma_{\mathrm{p}}} \\
&- \frac{1}{2jk_0}\left\langle \gamma_\tau\left(\frac{1}{\mu_r}\nabla\times\mathbf{v}_{\mathrm{m}}\right) + \alpha\gamma_\tau\left(\frac{1}{\mu_r}\nabla\times\mathbf{v}_{\mathrm{s}}\right), Z_p\left(\gamma_\tau\left(\frac{1}{\mu_r}\nabla\times\mathbf{u}_{\mathrm{m}}\right) + \alpha\gamma_\tau\left(\frac{1}{\mu_r}\nabla\times\mathbf{u}_{\mathrm{s}}\right)\right)\right\rangle_{\Gamma_{\mathrm{p}}} \\
&= -jk_0\eta(\mathbf{v}, \mathbf{J}^{\mathrm{imp}})_{\widetilde{\Omega}} + 2\sum_{i=1}^{2}\left\langle \pi_\tau(\mathbf{v}_i), \gamma_\tau(\nabla\times\mathbf{E}^{\mathrm{inc}})\right\rangle_{\overline{\Gamma_i}}.
\end{aligned} \tag{58}$$

Let us introduce a sesquilinear form, $a(\mathbf{v}, \mathbf{u})$ with both the trial and test functions, $\mathbf{u}$ and $\mathbf{v}$ in $\mathbf{H}(curl, \widetilde{\Omega})$, and write our Galerkin statement as:

Find $\mathbf{u} \in \mathbf{H}(curl, \widetilde{\Omega})$ such that

$$a(\mathbf{v}, \mathbf{u}) = f(\mathbf{v}), \quad \forall\mathbf{v} \in \mathbf{H}(curl, \widetilde{\Omega}) \tag{59}$$

with

$$\begin{aligned}
a(\mathbf{v}, \mathbf{u}) = &(\nabla\times\mathbf{v}, \frac{1}{\mu_r}\nabla\times\mathbf{u})_{\widetilde{\Omega}} - k_0^2(\mathbf{v}, \epsilon_r\mathbf{u})_{\widetilde{\Omega}} + \frac{1}{2}\left\langle \gamma_\tau\left(\frac{1}{\mu_r}\nabla\times\mathbf{v}_{\mathrm{m}}\right) - \alpha\gamma_\tau\left(\frac{1}{\mu_r}\nabla\times\mathbf{v}_{\mathrm{s}}\right), \pi_\tau(\mathbf{u}_{\mathrm{m}}) - \alpha\pi_\tau(\mathbf{u}_{\mathrm{s}})\right\rangle_{\Gamma_{\mathrm{p}}} \\
&+ \frac{1}{2}\left\langle \pi_\tau(\mathbf{v}_{\mathrm{m}}) - \alpha\pi_\tau(\mathbf{v}_{\mathrm{s}}), \gamma_\tau\left(\frac{1}{\mu_r}\nabla\times\mathbf{u}_{\mathrm{m}}\right) - \alpha\gamma_\tau\left(\frac{1}{\mu_r}\nabla\times\mathbf{u}_{\mathrm{s}}\right)\right\rangle_{\Gamma_{\mathrm{p}}} \\
&+ \frac{jk_0}{2}\left\langle \pi_\tau(\mathbf{v}_{\mathrm{m}}) - \alpha\pi_\tau(\mathbf{v}_{\mathrm{s}}), \frac{1}{Z_p}(\pi_\tau(\mathbf{u}_{\mathrm{m}}) - \alpha\pi_\tau(\mathbf{u}_{\mathrm{s}}))\right\rangle_{\Gamma_{\mathrm{p}}} \\
&- \frac{1}{2jk_0}\left\langle \gamma_\tau\left(\frac{1}{\mu_r}\nabla\times\mathbf{v}_{\mathrm{m}}\right) + \alpha\gamma_\tau\left(\frac{1}{\mu_r}\nabla\times\mathbf{v}_{\mathrm{s}}\right), Z_p\left(\gamma_\tau\left(\frac{1}{\mu_r}\nabla\times\mathbf{u}_{\mathrm{m}}\right) + \alpha\gamma_\tau\left(\frac{1}{\mu_r}\nabla\times\mathbf{u}_{\mathrm{s}}\right)\right)\right\rangle_{\Gamma_{\mathrm{p}}} \\
&+ 2\sum_{i=1}^{2}\left\langle \pi_\tau(\mathbf{v}_i), \gamma_\tau(k_0^2\mathbf{A}_{\mathrm{p}}(\mathbf{M}_i^{\mathbf{u}}) + \nabla\Phi_{\mathrm{p}}(\mathbf{M}_i^{\mathbf{u}}))\right\rangle_{\overline{\Gamma_i}},
\end{aligned} \tag{60}$$

and

$$f(\mathbf{v}) = -jk_0\eta(\mathbf{v}, \mathbf{J}^{\mathrm{imp}})_{\widetilde{\Omega}} + 2\sum_{i=1}^{2}\langle \pi_\tau(\mathbf{v}_i), \gamma_\tau(\nabla\times\mathbf{E}^{\mathrm{inc}})\rangle_{\overline{\Gamma_i}}. \tag{61}$$

2.4.3. Euler–Lagrange differential equation

Assuming that the weak solution $\mathbf{u}$ in Eq. (59) is smooth enough to permit the necessary integration by parts, we can rewrite (58) into the following form:

$$
\begin{aligned}
&\left(\mathbf{v}, \nabla\times\frac{1}{\mu_r}\nabla\times\mathbf{u} - k_0^2\epsilon_r\mathbf{u} + jk_0\eta\mathbf{J}^{\text{imp}}\right)_{\widetilde{\Omega}}\\
&+\frac{1}{2}\left\langle \gamma_\tau\left(\frac{1}{\mu_r}\nabla\times\mathbf{v}_{\text{m}}\right), \{\pi_\tau(\mathbf{u}_{\text{m}}) - \alpha\pi_\tau(\mathbf{u}_{\text{s}})\} - \frac{Z_p}{jk_0}\left\{\gamma_\tau\left(\frac{1}{\mu_r}\nabla\times\mathbf{u}_{\text{m}}\right) + \alpha\gamma_\tau\left(\frac{1}{\mu_r}\nabla\times\mathbf{u}_{\text{s}}\right)\right\}\right\rangle_{\Gamma_{\text{p}}}\\
&-\frac{\alpha^*}{2}\left\langle \gamma_\tau\left(\frac{1}{\mu_r}\nabla\times\mathbf{v}_{\text{s}}\right), \{\pi_\tau(\mathbf{u}_{\text{m}}) - \alpha\pi_\tau(\mathbf{u}_{\text{s}})\} + \frac{Z_p}{jk_0}\left\{\gamma_\tau\left(\frac{1}{\mu_r}\nabla\times\mathbf{u}_{\text{m}}\right) + \alpha\gamma_\tau\left(\frac{1}{\mu_r}\nabla\times\mathbf{u}_{\text{s}}\right)\right\}\right\rangle_{\Gamma_{\text{p}}}\\
&+\frac{1}{2}\left\langle \pi_\tau(\mathbf{v}_{\text{m}}), -\left\{\gamma_\tau\left(\frac{1}{\mu_r}\nabla\times\mathbf{u}_{\text{m}}\right) + \alpha\gamma_\tau\left(\frac{1}{\mu_r}\nabla\times\mathbf{u}_{\text{s}}\right)\right\} + \frac{jk_0}{Z_p}\{\pi_\tau(\mathbf{u}_{\text{m}}) - \pi_\tau(\mathbf{u}_{\text{s}})\}\right\rangle_{\Gamma_{\text{p}}}\\
&+\frac{\alpha^*}{2}\left\langle \pi_\tau(\mathbf{v}_{\text{s}}), -\left\{\gamma_\tau\left(\frac{1}{\mu_r}\nabla\times\mathbf{u}_{\text{m}}\right) + \alpha\gamma_\tau\left(\frac{1}{\mu_r}\nabla\times\mathbf{u}_{\text{s}}\right)\right\} - \frac{jk_0}{Z_p}\{\pi_\tau(\mathbf{u}_{\text{m}}) - \alpha\pi_\tau(\mathbf{u}_{\text{s}})\}\right\rangle_{\Gamma_{\text{p}}}\\
&+\sum_{i=1}^{2}\langle\pi_\tau(\mathbf{v}_i), \gamma_\tau(\nabla\times\mathbf{u}_i) + 2\gamma_\tau(k_0^2\mathbf{A}_{\text{p}}(\mathbf{M}_i) + \nabla_\tau\Phi_{\text{p}}(\mathbf{M}_i) - \nabla\times\mathbf{E}^{\text{inc}})\rangle_{\overline{\Gamma_i}} = 0.
\end{aligned}
\tag{62}
$$

Since Eq. (62) holds true for all $\mathbf{v}\in\mathbf{H}(curl,\widetilde{\Omega})$, subsequently, we have the following Euler–Lagrange equations in $\widetilde{\Omega}$ and boundary conditions on Γ_{p} and $\overline{\Gamma_i}$, $i=1,2$:

$$
\begin{aligned}
&\nabla\times\frac{1}{\mu_r}\nabla\times\mathbf{u} - k_0^2\epsilon_r\mathbf{u} = -jk_0\eta\mathbf{J}^{\text{imp}} \quad \text{in } \widetilde{\Omega},\\
&\gamma_\tau\left(\frac{1}{\mu_r}\nabla\times\mathbf{u}_{\text{m}}\right) + \frac{jk_0}{Z_p}\pi_\tau(\mathbf{u}_{\text{m}}) = -\alpha\gamma_\tau\left(\frac{1}{\mu_r}\nabla\times\mathbf{u}_{\text{s}}\right) + \frac{jk_0}{Z_p}\alpha\pi_\tau(\mathbf{u}_{\text{s}}) \quad \text{on } \Gamma_{\text{p}},\\
&\gamma_\tau\left(\frac{1}{\mu_r}\nabla\times\mathbf{u}_{\text{m}}\right) - \frac{jk_0}{Z_p}\pi_\tau(\mathbf{u}_{\text{m}}) = -\alpha\gamma_\tau\left(\frac{1}{\mu_r}\nabla\times\mathbf{u}_{\text{s}}\right) - \frac{jk_0}{Z_p}\alpha\pi_\tau(\mathbf{u}_{\text{s}}) \quad \text{on } \Gamma_{\text{p}},\\
&\gamma_\tau(\nabla\times\mathbf{u}_i) = 2\gamma_\tau(k_0^2\mathbf{A}_{\text{p}}(\mathbf{M}_i) + \nabla_\tau\Phi_{\text{p}}(\mathbf{M}_i) - \nabla\times\mathbf{E}^{\text{inc}}) \quad \text{on } \overline{\Gamma_i},\ i=1,2.
\end{aligned}
\tag{63}
$$

About Eq. (63), we should make three remarks:

1. It is obvious that Eq. (63) is equivalent to the BVP described in (33)–(37) for the unit cell;
2. However, in (63), we have replaced the more conventional Dirichlet and Neumman type boundary conditions in (35) and (36) with the Robin type boundary conditions. In the finite dimensional discretizations, this strategy proves beneficial as shown in references [18,19]. We shall also elaborate this point further in the numerical results section;
3. In this exercise, we have also realized that through the choices of coefficients, p and q, in the IP formulation, different types of transmission conditions can be readily incorporated.

2.5. Constraints on the corner edges

The boundary integrals (over $\overline{\Gamma_i}$) in (58) still need to be addressed further. Note that, in its current form, the second term, $\langle\pi_\tau(\mathbf{v}_i), \gamma_\tau(\nabla_\tau\Phi_{\text{p}}(\mathbf{M}_i))\rangle_{\overline{\Gamma_i}}$, will not be symmetric and is also not very convenient for implementation. To mitigate these difficulties, we shall perform integration by part, and write

$$
\begin{aligned}
\langle\pi_\tau(\mathbf{v}_i), \gamma_\tau(\nabla_\tau\Phi_{\text{p}}(\mathbf{M}_i))\rangle_{\overline{\Gamma_i}} &:= \int_{\overline{\Gamma_i}}\pi_\tau(\mathbf{v}_i)(\mathbf{r})\cdot\mathbf{n}_i\times\nabla_\tau\left\{\int_{\overline{\Gamma_i}}G_{\text{p}}(\mathbf{r},\mathbf{r}')(\nabla'_\tau\cdot\mathbf{M}_i^{\mathbf{u}})(\mathbf{r}')d\mathbf{S}'\right\}d\mathbf{S}\\
&= -\int_{\overline{\Gamma_i}}(\nabla_\tau\cdot\mathbf{M}_i^{\mathbf{v}})(\mathbf{r})\left\{\int_{\overline{\Gamma_i}}G_{\text{p}}(\mathbf{r},\mathbf{r}')(\nabla'_\tau\cdot\mathbf{M}_i^{\mathbf{u}})(\mathbf{r}')d\mathbf{S}'\right\}d\mathbf{S} + \int_{\overline{\Gamma_i}\bigcap\Gamma_{\text{m}}}(\mathbf{M}_i^{\mathbf{v}}\cdot\mathbf{n}_{\text{m}})(\mathbf{r})\Phi_{\text{p,m}}(\mathbf{M}_i^{\mathbf{u}})(\mathbf{r})dl\\
&\quad + \int_{\overline{\Gamma_i}\bigcap\Gamma_{\text{s}}}(\mathbf{M}_i^{\mathbf{v}}\cdot\mathbf{n}_{\text{s}})(\mathbf{r})\Phi_{\text{p,s}}(\mathbf{M}_i^{\mathbf{u}})(\mathbf{r})dl,
\end{aligned}
\tag{64}
$$

with $\Phi_{\text{p,m}}^{\mathbf{u}}(\mathbf{r})$ and $\Phi_{\text{p,s}}^{\mathbf{u}}(\mathbf{r})$ denote $\Phi_{\text{p}}^{\mathbf{u}}(\mathbf{r})$ with $\mathbf{r}\in\overline{\Gamma_i}\bigcap\Gamma_{\text{m}}$ and $\mathbf{r}\in\overline{\Gamma_i}\bigcap\Gamma_{\text{s}}$, respectively. Moreover, the scalar potential, $\Phi_{\text{p}}(\mathbf{M}_i^{\mathbf{u}})$ is periodic and hence it satisfies the periodic relationship $\Phi_{\text{p,m}}(\mathbf{M}_i^{\mathbf{u}})(\mathbf{r}) = \alpha\Phi_{\text{p,s}}(\mathbf{M}_i^{\mathbf{u}})(\mathbf{r}+\mathbf{D})$, where $\mathbf{D}$ is either $D_x\mathbf{x}$ or $D_y\mathbf{y}$. Hence, the contour integrals in (64) can be combined to give the following expression:

$$
\begin{aligned}
&\int_{\overline{\Gamma_i}\bigcap\Gamma_{\text{m}}}(\mathbf{M}_i^{\mathbf{v}}\cdot\mathbf{n}_{\text{m}})(\mathbf{r})\Phi_{\text{p,m}}(\mathbf{M}_i^{\mathbf{u}})(\mathbf{r})dl + \int_{\overline{\Gamma_i}\bigcap\Gamma_{\text{s}}}(\mathbf{M}_i^{\mathbf{v}}\cdot\mathbf{n}_{\text{s}})(\mathbf{r})\Phi_{\text{p,s}}(\mathbf{M}_i^{\mathbf{u}})(\mathbf{r})dl\\
&= \int_{\overline{\Gamma_i}\bigcap\Gamma_{\text{m}}}[(\mathbf{M}_{i,\text{m}}^{\mathbf{v}}(\mathbf{r}) - \alpha\mathbf{M}_{i,\text{s}}^{\mathbf{v}}(\mathbf{r}+\mathbf{D}))\cdot\mathbf{n}_{\text{m}}]^*\Phi_{\text{p,m}}(\mathbf{r})dl.
\end{aligned}
\tag{65}
$$

Then, it is clear that in order for the contour integrals to vanish, we shall have to impose the periodic constraint, on both the trial and test fields, $\pi_\tau(\mathbf{u}_{\text{m}})|_{\overline{\Gamma_i}\bigcap\Gamma_{\text{m}}} = \alpha\pi_\tau(\mathbf{u}_{\text{s}})|_{\overline{\Gamma_i}\bigcap\Gamma_{\text{s}}}$. Consequently, the Galerkin statement in (59) needs to be modified slightly to reflect this constraint. Namely,

Find $\mathbf{u} \in \mathbf{X} \subset \mathbf{H}(curl, \widetilde{\Omega})$ such that $a(\mathbf{v}, \mathbf{u}) = f(\mathbf{v}), \quad \forall \mathbf{v} \in \mathbf{X}$

and the function space $\mathbf{X}$ is defined as:

$$\mathbf{X} := \{\mathbf{v} \in \mathbf{H}(curl, \widetilde{\Omega}), \pi_\tau(\mathbf{v}_m)|_{\overline{\Gamma_i} \bigcap \Gamma_m} = \alpha \pi_\tau(\mathbf{v}_s)|_{\overline{\Gamma_i} \bigcap \Gamma_s}\}. \tag{66}$$

2.6. Periodic Green's function

In this section, we briefly discuss the expression for the periodic Green's function used in this work. Assume that the boundary element surface $\overline{\Gamma_i}$ is flat and resides on x–y plane. Moreover, the periodicity in x and y-directions are D_x, and D_y, respectively. Subsequently, we employ the following Ewald transformation for fast evaluations of the periodic Green's function [22,9]:

$$G_p(\mathbf{r}, \mathbf{r}') = G_{p1}(\mathbf{r}, \mathbf{r}') + G_{p2}(\mathbf{r}, \mathbf{r}'), \tag{67}$$

where

$$\begin{aligned} G_{p1}(\mathbf{r}, \mathbf{r}') &= \sum_{m=-\infty}^{\infty} \sum_{n=-\infty}^{\infty} \frac{e^{-j\mathbf{k}_{tmn} \cdot (\mathbf{r} - \mathbf{r}')}}{2jAk_{zmn}} \operatorname{erfc}\left(\frac{jk_{zmn}}{2E_{opt}}\right), \\ G_{p2}(\mathbf{r}, \mathbf{r}') &= \sum_{m=-\infty}^{\infty} \sum_{n=-\infty}^{\infty} \frac{e^{-j\mathbf{k}_t \cdot \boldsymbol{\rho}_{mn}}}{8\pi R_{mn}} \left[e^{-jk_0 R_{mn}} \operatorname{erfc}\left(R_{mn} E_{opt} - \frac{jk_0}{2E_{opt}}\right) + e^{-jk_0 R_{mn}} \operatorname{erfc}\left(R_{mn} E_{opt} + \frac{jk_0}{2E_{opt}}\right) \right] \end{aligned} \tag{68}$$

In (68), A is the area of $\overline{\Gamma_i}$, and

$$\boldsymbol{\rho}_{mn} = mD_x \mathbf{x} + nD_y \mathbf{y}, \tag{69}$$

$$R_{mn} = |\mathbf{r} - \mathbf{r}' - \boldsymbol{\rho}_{mn}|, \tag{70}$$

$$\mathbf{k}_{tmn} = \mathbf{k}_t + \frac{2\pi m}{D_x} \mathbf{x} + \frac{2\pi n}{D_y} \mathbf{y}, \tag{71}$$

$$k_{zmn} = \sqrt{k_0^2 - \mathbf{k}_t \cdot \mathbf{k}_t}, \tag{72}$$

$$E_{opt} = \sqrt{\frac{2\pi}{A}}. \tag{73}$$

The complementary error function "erfc" is also defined as.

$$\operatorname{erfc}(x) = \frac{2}{\sqrt{\pi}} \int_x^\infty e^{-u^2} du. \tag{74}$$

3. Finite dimensional implementation

3.1. Discrete Galerkin formulation

In the practical implementation, we shall first partition the unit cell domain $\widetilde{\Omega}$ into a finite element mesh, $\widetilde{\Omega}^h$, which is formed with tetrahedral elements, K. Assuming that the tetrahedral mesh is regular, namely, the tetrahedral elements are similar and with the largest diameter of h. A popular set of curl-conforming basis functions is the Nédélec elements, and in this work, we have adopted the first type of Nédélec elements. Particularly, we have employed the $\mathcal{N}_1^l$ (see reference [25]) basis functions.

We are now ready to state formally our discrete Galerkin formulation as:

Find $\mathbf{u}^h \in \mathbf{X}^h \subset \mathbf{V}^h$ such that $a(\mathbf{v}^h, \mathbf{u}^h) = f(\mathbf{v}^h), \forall \mathbf{v} \in \mathbf{X}^h$.

where the two finite dimensional subspaces are defined as:

$$\begin{aligned} \mathbf{V}^h &= \{\mathbf{v}^h \in \mathbf{H}(curl, \widetilde{\Omega}), \mathbf{v}^h|_K, \nabla \times \mathbf{v}^h|_K \in (P^1(K))^3\}, \\ \mathbf{X}^h &= \{\mathbf{v}^h \in \mathbf{V}^h, \int_{\Gamma_i \bigcap \Gamma_m} (\mathbf{w}_{i,m}^h \cdot \hat{\mathbf{t}})((\mathbf{v}_{i,m} - \alpha \mathbf{v}_{i,s}) \cdot \hat{\mathbf{t}}) dl = 0, \forall \mathbf{w}^h \in \mathbf{V}^h\}, \end{aligned} \tag{75}$$

where $P^1(K)$ is the set of linear polynomials defined in the element K.

3.2. Preconditioner

In this work, hierarchical higher order basis functions ($p = 2$) are used. Therefore, the matrix resulting from (59) (denoted A herein) can be partitioned in terms of the basis order as

$$A = \begin{bmatrix} A_{11} & A_{12} \\ A_{21} & A_{22} \end{bmatrix}. \tag{76}$$

Through this partition, p-type multiplicative Schwarz preconditioner (pMUS) [26,27] can be applied in the solution process. A 2×2 matrix can be written in a product form as

$$A = \begin{bmatrix} A_{11} & A_{12} \\ A_{21} & A_{22} \end{bmatrix} = \begin{bmatrix} I_1 & 0 \\ A_{21}A_{11}^{-1} & I_2 \end{bmatrix} \begin{bmatrix} A_{11} & 0 \\ 0 & A_{22} - A_{21}A_{11}^{-1}A_{12} \end{bmatrix} \begin{bmatrix} I_1 & A_{11}^{-1}A_{12} \\ 0 & I_2 \end{bmatrix}, \tag{77}$$

and its inverse can be easily found as

$$A^{-1} = \begin{bmatrix} I_1 & -A_{11}^{-1}A_{12} \\ 0 & I_2 \end{bmatrix} \begin{bmatrix} A_{11}^{-1} & 0 \\ 0 & \left(A_{22} - A_{21}A_{11}^{-1}A_{12}\right)^{-1} \end{bmatrix} \begin{bmatrix} I_1 & 0 \\ -A_{21}A_{11}^{-1} & I_2 \end{bmatrix}. \tag{78}$$

The above expression involves inversion of the first order block (A_{11}) and the Schur complement ($S = A_{22} - A_{21}A_{11}^{-1}A_{12}$). For an efficient computation, we first approximate the Schur complement by $S \approx A_{22}$, and secondly perform incomplete LU (ILU) factorization of the sub-blocks A_{11} and A_{22}. Namely,

$$A_{11} = \widetilde{L}_1\widetilde{U}_1 + E_1, \quad \|E_1\| \leqslant 10^{-6}, \tag{79}$$

$$A_{22} = \widetilde{L}_2\widetilde{U}_2 + E_2. \quad \|E_2\| \leqslant 10^{-3}. \tag{80}$$

Finally, the pMUS preconditioner M^{-1} can be constructed as

$$M^{-1} = \begin{bmatrix} I_1 & -(\widetilde{L}_1\widetilde{U}_1)^{-1}A_{12} \\ 0 & I_2 \end{bmatrix} \begin{bmatrix} (\widetilde{L}_1\widetilde{U}_1)^{-1} & 0 \\ 0 & (\widetilde{L}_2\widetilde{U}_2)^{-1} \end{bmatrix} \begin{bmatrix} I_1 & 0 \\ -A_{21}(\widetilde{L}_1\widetilde{U}_1)^{-1} & I_2 \end{bmatrix}. \tag{81}$$

This preconditioner can be efficiently applied in each iteration of an iterative solver without an explicit assembly process. Also, the efficiency and the effectiveness of the pMUS preconditioner can be observed in [26,27].

4. Numerical examples

Throughout the numerical studies presented herein this section, the average relative impedance for the periodic boundary, Γ_p, is set to be $Z_p = 1$.

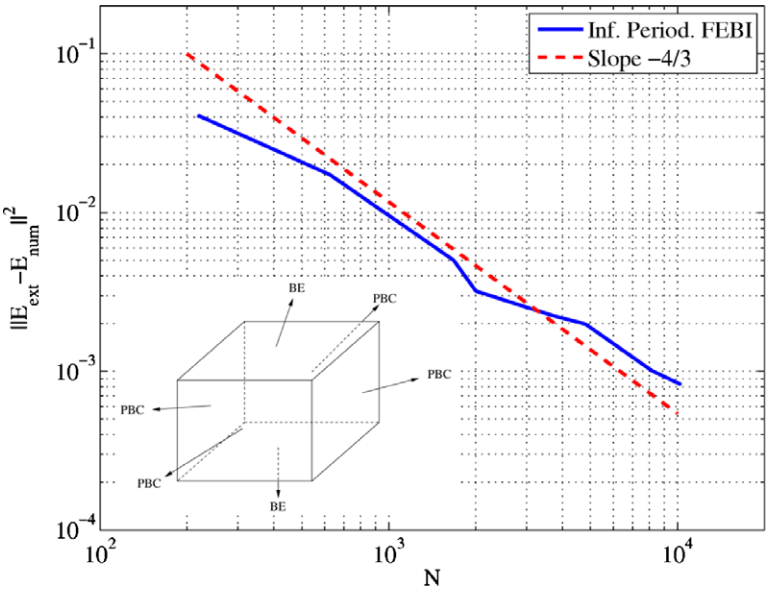

Fig. 3. The error rate-of-convergence of the solution with the mesh refinement.

4.1. Convergence study

The convergence of the solution with the mesh refinement was measured for an empty unit cell. A plane wave incident field was imposed for convenient computation of the exact solution. In Fig. 3, the square of the norm of the electric field error is plotted versus the number of unknowns. The numerical errors (with $p = 2$) in the h-version of mesh refinements for classical finite element method is proportional to $O(h^4) = O\left(N^{-\frac{4}{3}}\right)$, and a corresponding slope is also plotted in Fig. 3 for the comparison. Obviously, an optimal rate of convergence is achieved by the proposed method with the choice of the coefficients discussed in Section 2.4.2.

4.2. Patch antenna array

For verification of the proposed method, an infinite microstrip patch array was analyzed. The unit cell geometry is shown in Fig. 4. This problem was previously analyzed by Pozar and Schaumbert in [6] and McGrath and Pyati in [8]. For each scanning direction, the normalized active reflection coefficient was computed through

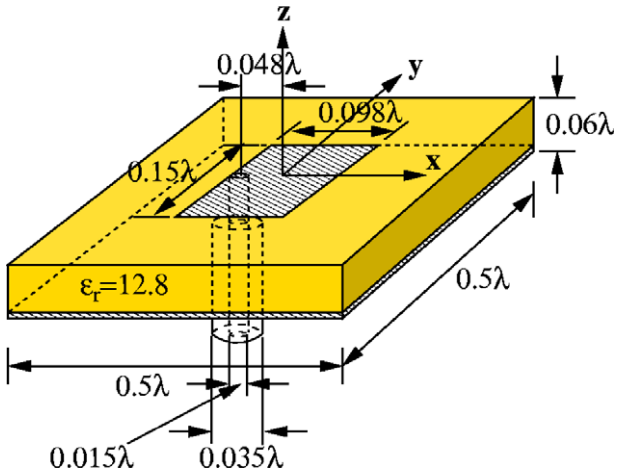

Fig. 4. The unit cell geometry of a microstrip patch array.

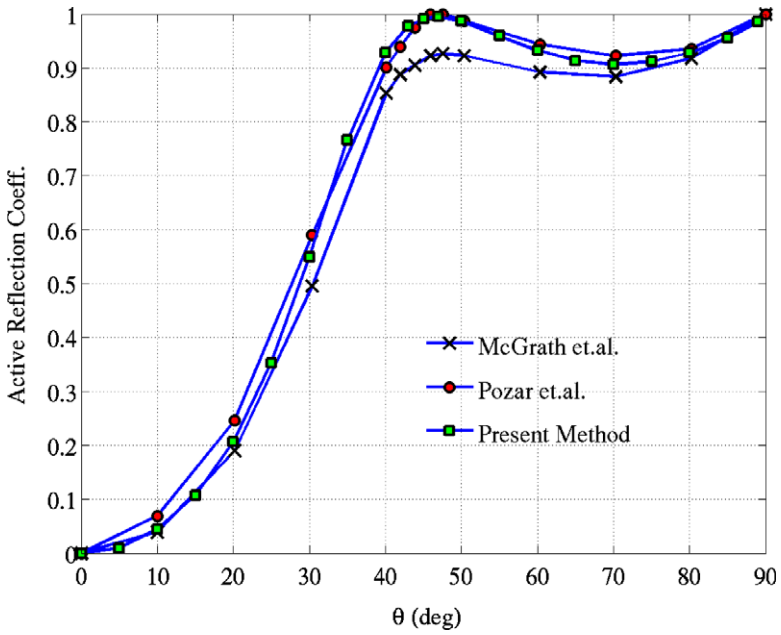

Fig. 5. The active reflection coefficient of a microstrip patch array for E-plane scanning.

$$R(\vartheta,\varphi)=\left|\frac{Z_{in}(\vartheta,\varphi)-Z_{in}(0,0)}{Z_{in}(\vartheta,\varphi)+Z_{in}(0,0)}\right|. \tag{82}$$

By the normalization, the matching network for the broadside scan is numerically realized. Fig. 5 shows the active reflection coefficients versus E-plane (x–z plane) scanning. The figure shows reasonable agreement between previous works [6,8] and the proposed method.

The convergence of the iterative solver is also studied in this example. The generalized conjugate residual (GCR) method is used as an iterative solver in this work, and the convergence behavior of the Robin type TC used in this paper is compared to the classical Dirichlet and Neumann type TC. As indicated in Section 2.4.3, the choice of the coefficients in Section 2.4.2

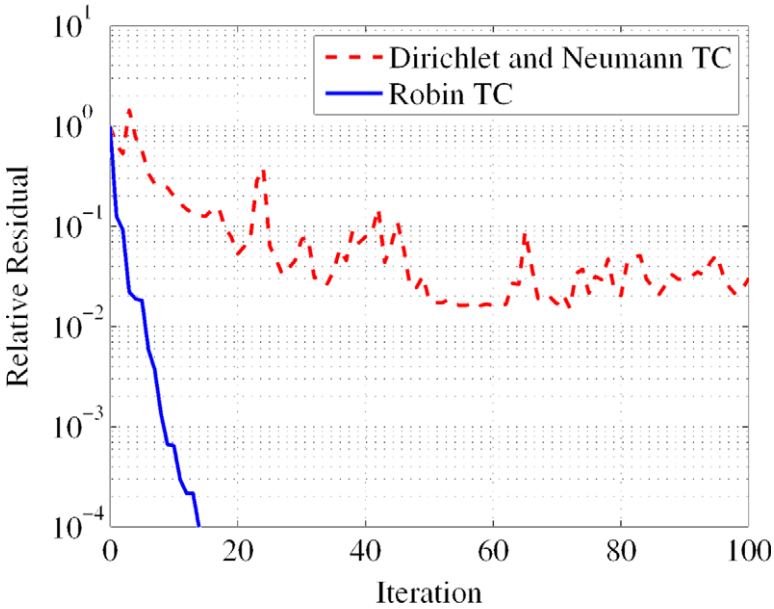

Fig. 6. The convergence of GCR by different TCs for broadside scanning of a microstrip patch array.

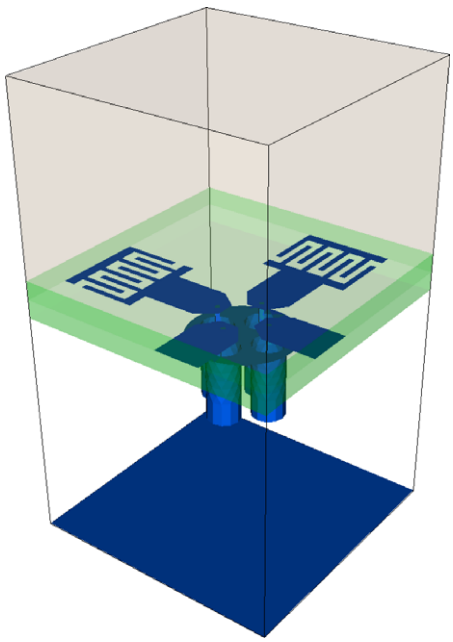

Fig. 7. The unit cell geometry of a ultra wide band antenna array.

results in a Robin TC, whereas $p = 0$ and $q = 0$ result in a Dirichlet and Neumann type TC. For the broadside scanning, the convergence by each TC was obtained and plotted in Fig. 6. The benefit of the Robin TC is clearly demonstrated by this experiment.

4.3. Ultra wide band antenna array

The next example is an ultra wide band antenna array. The design concept of this antenna is given in [1] where the dipole elements are configured to operate at broad range of frequencies. The geometry of the unit cell is shown in Fig. 7 and the detailed dimensions can be found in Fig. 8. Two orthogonal sets of dipoles loaded with finger capacitors are fed by the feed organizer (see [1] Chapter 10). In this work, a simplified feed organizer model is used as shown in Fig. 9, which consists of four coaxial transmission lines sharing a common ground, and providing the improved matching explained in [1]. One dipole element in the unit cell was excited at the frequencies in 2–20GHz, and the broadside radiation was considered in this simulation. The electric field magnitude at 10 GHz is shown in Fig. 10. The input impedances normalized to 100 Ω at the operating frequency range were computed and plotted on the Smith chart in Fig. 11. In the figure, the result from the HFSS is also provided for the comparison, and reasonable agreement between proposed method and the HFSS can be observed.

4.4. Meander line polarizer

In this section, a meander line polarizer [1] is analyzed. This polarizer converts a linearly polarized wave into a circularly polarized wave. The unit cell geometry is presented in Fig. 12, and the details of the geometrical configuration can be found

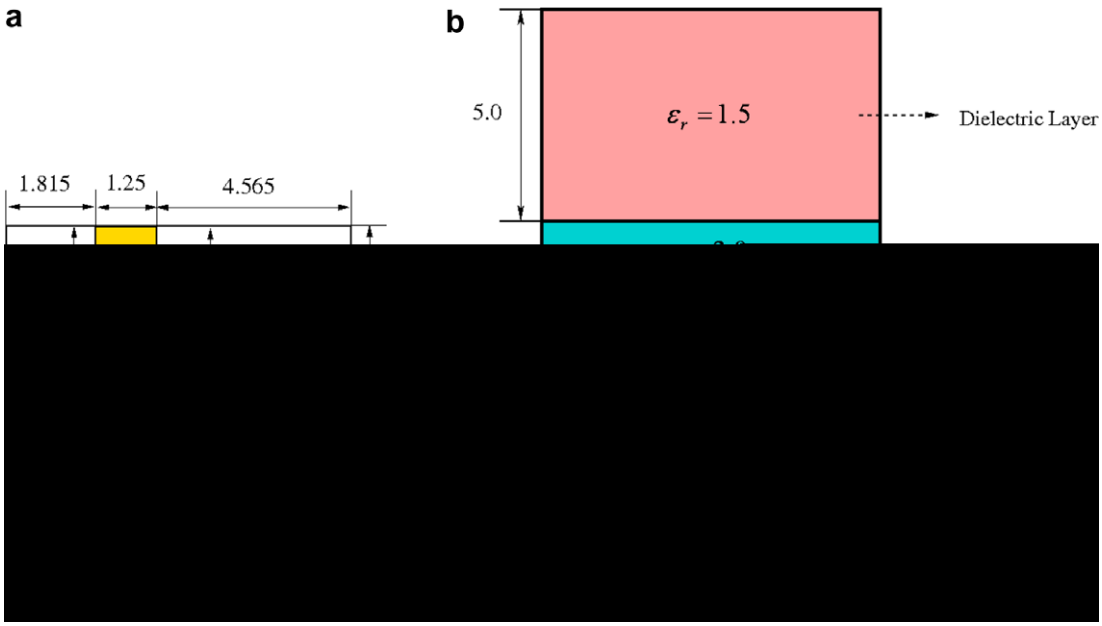

Fig. 8. The dimensions of the ultra wide band antenna in the unit cell (the unit is *mm*): (a) top view and (b) side view.

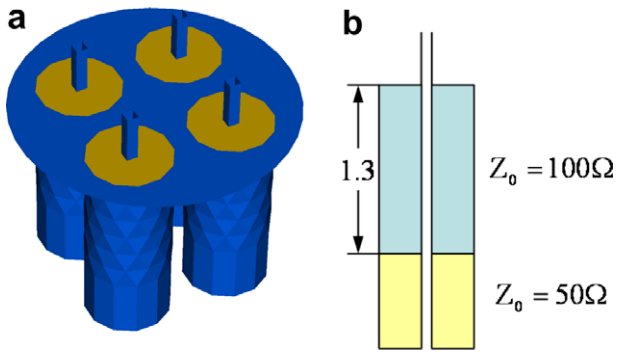

Fig. 9. The feed organizer: (a) 3D view and (b) cross section of each coaxial transmission line. (*mm* in unit)

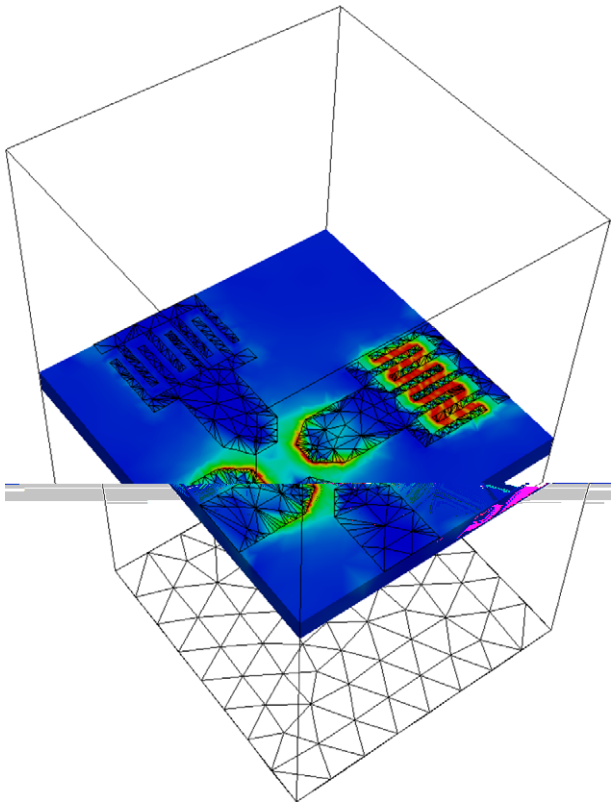

Fig. 10. The electric field distribution in the unit cell of a ultra wide band antenna array at 10 GHz.

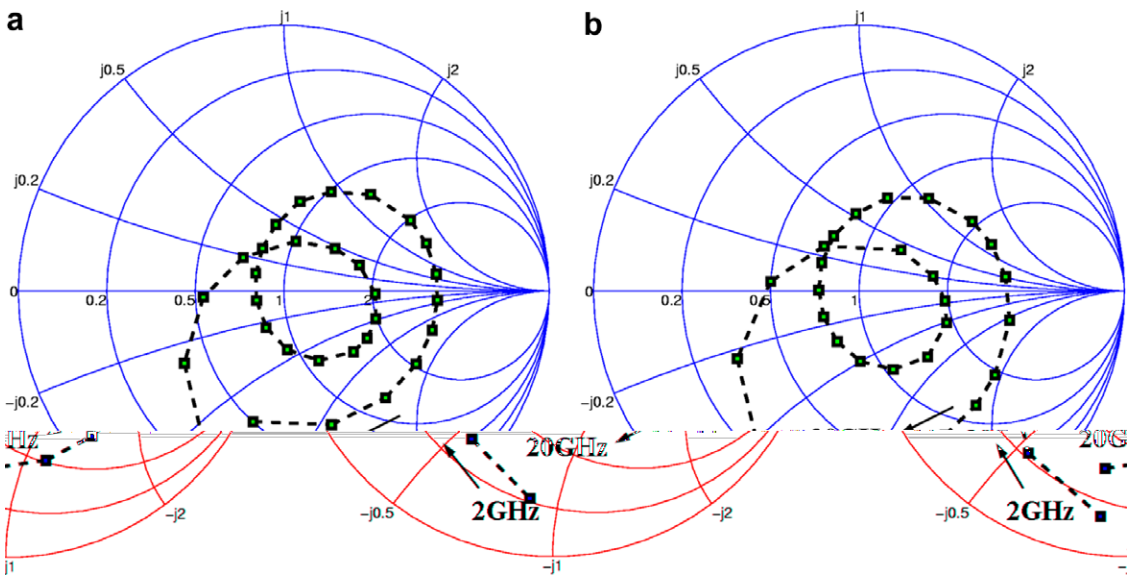

Fig. 11. S-parameters of the ultra wide band antenna array: (a) proposed method and (b) HFSS.

in Fig. 13. The incident wave was imposed on one side of the geometry, and the transmitted field was measured on the other side. The incident field is linearly polarized, and therefore the transmitted field is expected to be circularly polarized. To observe the circular polarization, the transmitted field was decomposed into co-polarized and cross-polarized components, and the magnitude and phase between two components were compared. For a circularly polarized field, the magnitude ratio should be one while the phase difference should be 90°. The lowest, TE_{00}, Floquet mode was imposed as the incident field

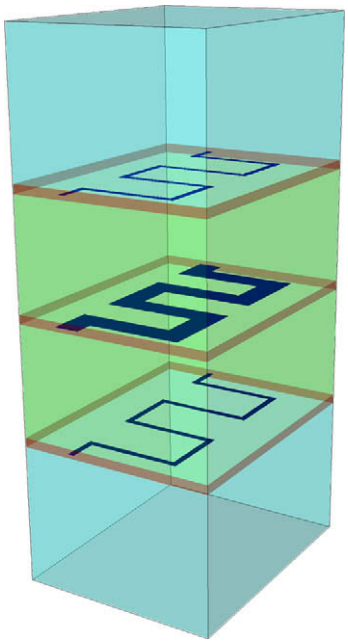

Fig. 12. The unit cell geometry of a meander line polarizer.

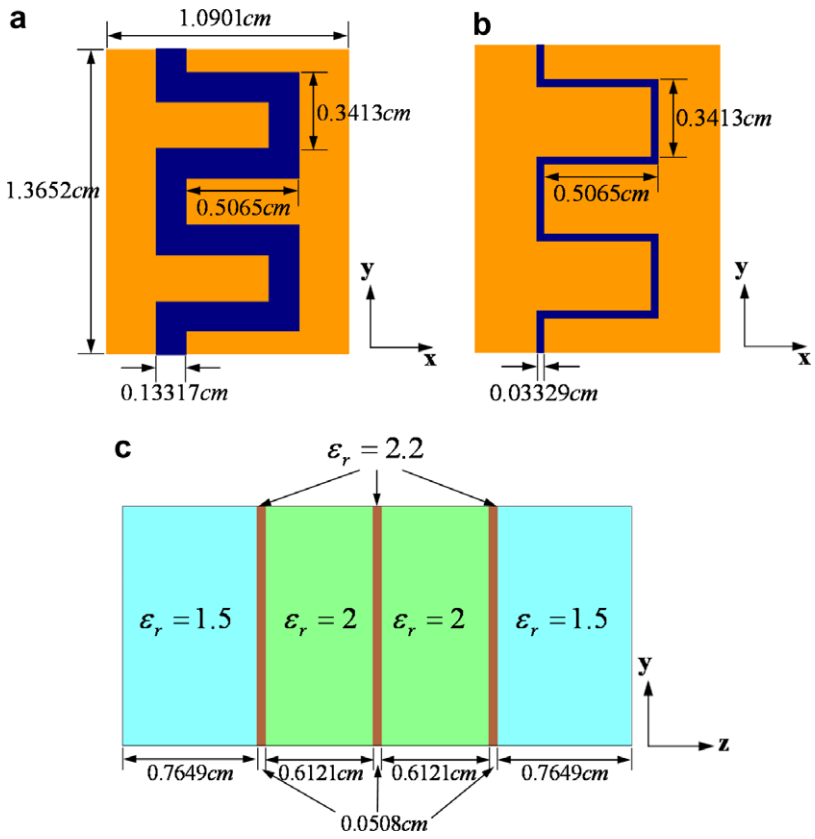

Fig. 13. The dimensions of the meander line in the unit cell: (a) center meander line; (b) outer meander line; and (c) side view.

along with the incident angle $\theta = 0^\circ,\ 45^\circ$ and 60° $(\phi = 45^\circ)$. The simulation result is shown in Fig. 14, where the circularly polarized field can be expected up to the frequency 8.5 GHz regardless of the incident angle.

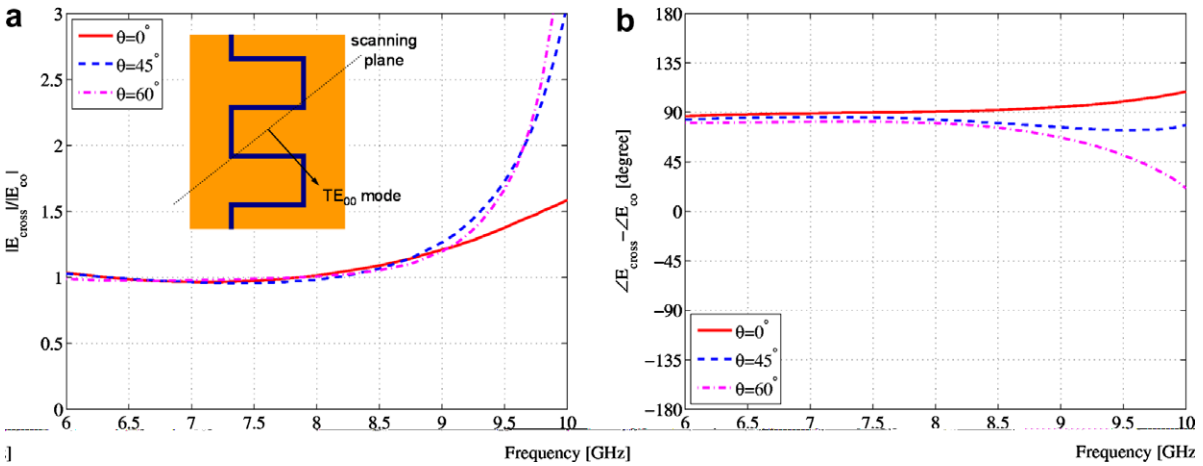

Fig. 14. The comparison of the transmitted co-polarized and cross-polarized fields: (a) magnitude ratio and (b) phase difference in degree.

5. Conclusions

A finite element/boundary element method for periodic structures was proposed. The formulation was derived through an interior penalty approach, which allowed non-periodic meshes for the discretization of the unit cell. Additional Dirichlet conditions were added for the non-conformity of the boundary elements between the adjacent unit cells. The acceleration of the boundary element assembly was achieved by the efficient computation of the periodic Green's function through the Ewald transformation. The formulation was shown to provide an optimal rate of convergence in the solution. The Robin transmission conditions were shown to give improved iterative solver convergence over a formulation with simple Dirichlet and Neumann boundary conditions.

Acknowledgment

The authors thank the Northrop Grumman Corporation for their interest and support of this study.

References

[1] B. Munk, Finite Antenna Arrays and FSS, John Wiley & Sons, New York, 2003.
[2] S. Kasturi, D.H. Schaubert, Effect of dielectric permittivity on infinite arrays of single-polarized Vivaldi antennas, IEEE Trans. Antennas Propagat. 54 (2) (2006) 351–358.
[3] J. Romeu, Y. Rahmat-Samii, Fractal FSS: a novel dual-band frequency selective surface, IEEE Trans. Antennas Propagat. 48 (7) (2000) 1097–1105.
[4] J.B. Pendry, Negative refraction, Contemp. Phys. 45 (3) (2004) 191–202.
[5] V. Eleftheriades, G.A.K. Iyer, P.C. Kremer, Planar negative refractive index media using periodically L-C loaded transmission lines, IEEE Trans. Microwave Theory Technol. 50 (12) (2002) 2702–2712.
[6] D.M. Pozar, D.H. Schaubert, Analysis of an infinite array of rectangular microstrip patches with idealized probe feeds, IEEE Trans. Antennas Propagat. 32 (1984) 1101–1107.
[7] J.-M. Jin, J.L. Volakis, Scattering and radiation analysis of three-dimensional cavity arrays via a hybrid finite-element method, IEEE Trans. Antennas Propagat. 41 (11) (1993) 1580–1586.
[8] D.T. McGrath, V.P. Pyati, Phased array antenna analysis with the hybrid finite element method, IEEE Trans. Antennas Propagat. 42 (4) (1994) 1625–1630.
[9] T.F. Eibert, J.L. Volakis, D.R. Wilton, D.R. Jackson, Hybrid FE/BI modeling of 3-D doubly periodic structures utilizing triangular prismatic elements and an MPIE formulation accelerated by Ewald transformation, IEEE Trans. Antennas Propagat. 47 (5) (1999) 843–849.
[10] L.E.R. Petersson, J.-M. Jin, A three-dimensional time-domain finite-element formulation for periodic structures, IEEE Trans. Antennas Propagat. 54 (1) (2006) 12–19.
[11] M.N. Vouvakis, K. Zhao, J.-F. Lee, Finite-element analysis of infinite periodic structures with nonmatching triangulations, IEEE Trans. Magn. 42 (4) (2006) 691–694.
[12] d.l.R. Valentin, J. Zapata, M.A. Gonzalez, Finite element analysis of periodic structures without constrained meshes, IEEE Trans. Antennas Propagat. 56 (9) (2008) 3020–3028.
[13] G.A. Baker, Finite element methods for elliptic equations using nonconforming elements, Math. Comput. 31 (1977) 45–59.
[14] M.F. Wheeler, An elliptic collocation-finite element method with interior penalties, SIAM J. Numer. Anal. 15 (1) (1978) 152–161.
[15] D. Arnold, An interior penalty finite element method with discontinuous elements, SIAM J. Numer. Anal. 19 (4) (1982) 742–760.
[16] I. Perugia, D. Schötzau, P. Monk, Stabilized interior penalty methods for time-harmonic Maxwell equations, Comput. Methods Appl. Mech. Eng. 191 (2-5) (2002) 4675–4697.
[17] P. Houston, I. Perugia, A. Schneebeli, D. Schötzau, Interior penalty method for the indefinite time-harmonic Maxwell equations, Numer. Math. 100 (3) (2005) 485–518.
[18] B. Després, P. Joly, J. Roberts, A domain decomposition method for the harmonic Maxwell equations, in: Iterative Methods in Linear Algebra (Brussels, 1991), North-Holland, Amsterdam, 1992, pp. 475–484.
[19] S.-C. Lee, M. Vouvakis, J.-F. Lee, A non-overlapping domain decomposition method with non-matching grids for modeling large finite antenna arrays, J. Comput. Phys. 203 (1) (2005) 1–21.

[20] A.F. Peterson, Absorbing boundary conditions for the vector wave equation, Microwave Opt. Technol. Lett. 1 (1988) 62–64.
[21] Z.S. Sacks, D.M. Kingsland, R. Lee, J.-F. Lee, A perfectly matched anisotropic absorber for use as an absorbing boundary condition, IEEE Trans. Antennas Propagat. 43 (12) (1995) 1460–1463.
[22] K.E. Jordan, G.R. Richter, P. Sheng, An efficient numerical evaluation of the Green's function for the Helmholtz operator on periodic structures, J. Comput. Phys. 63 (1986) 222–235.
[23] J.-C. Nèdélec, Acoustic and electromagnetic equations, integral representations for harmonic problems, Applied Mathematical Sciences, vol. 144, Springer-Verlag, New York, 2001.
[24] D. Arnold, F. Brezzi, B. Cockburn, L. Marini, Unified analysis of discontinuous Galerkin methods for elliptic problems, SIAM J. Numer. Anal. 39 (5) (2002) 1749–1779.
[25] J. Schoberl, Numerical methods for Maxwell's equations, Lecture Note, <http://www.hpfem.jku.at>.
[26] J.-F. Lee, D.-K. Sun, p-Type multiplicative Schwarz (pMUS) method with vector finite elements for modeling three-dimensional waveguide discontinuities, IEEE Trans. Microwave Theory Technol. 52 (3) (2004) 864–870.
[27] D.K. Sun, J.-F. Lee, Z.J. Cendes, Construction of nearly orthogonal Nedelec bases for rapid convergence with multilevel preconditioned solvers, SIAM J. Sci. Comput. 23 (4) (2001) 1053–1076.